El Niño key driver of drought in highly vulnerable Southern African countries

Authors

Joyce Kimutai, *Grantham Institute, Imperial College London, UK*
Mariam Zachariah, *Grantham Institute, Imperial College London, UK*
Bernardino Nhantumbo, *National Institute of Meteorology, Maputo, Mozambique*
Tiro Nkemelang, *Botswana Institute for Technology Research and Innovation, Gaborone, Botswana, African Climate and Development Initiative, University of Cape Town, Cape Town, South Africa*
Suman Jain*, Mathematics and Statistics Department, University of Zambia,Zambia*
Izidine Pinto, *Royal Netherlands Meteorological Institute (KNMI), De Bilt, The Netherlands*
Ben Clarke, *Grantham Institute, Imperial College London, UK*
Piotr Wolski, *Climate System Analysis Group, University of Cape Town, Cape Town, South Africa*
Maja Vahlberg, *Red Cross Red Crescent Climate Centre, the Hague, Netherlands (based in Ubmeje/Umeå, Sweden)*
Tesse de Boer, *Red Cross Red Crescent Climate Centre, the Hague, Netherlands (based in Amsterdam, Netherlands)*
Simphiwe Stewart, *Red Cross Red Crescent Climate Centre, the Hague, Netherlands (based in Amsterdam, Netherlands)*
Ireen Mutombwa, *South African Red Cross Society, Randburg, South Africa (based in Johannesburg, South Africa)*
Wina Wina, *Zambia Red Cross Society, Lusaka, Zambia*
Roop Singh, *Red Cross Red Crescent Climate Centre, the Hague, Netherlands (based in New Jersey, USA)*
Julie Arrighi, *Red Cross Red Crescent Climate Centre, the Hague, Netherlands (based in New York, USA)*
Friederike E. L Otto, *Grantham Institute, Imperial College London, UK*

Review authors

Sjoukje Philip, *Royal Netherlands Meteorological Institute (KNMI), De Bilt, The Netherlands;*
Ben Clarke, *Grantham Institute, Imperial College London, UK*

Main findings

- Reliance on rain-fed subsistence crop production and drought-sensitive water sources result in chronic high vulnerability to rainfall anomalies, and limited coping capacity.
- Multiple drivers contributed to the currently high, and rising, food insecurity and malnutrition levels including several years with high food prices, ongoing recovery from floods, as well as agricultural pests and diseases.
- High deforestation rates are a major driver of environmental degradation across the countries, exacerbating risk and impacts associated with drought.
- Using four different observational data products we find that droughts such as this one are expected to happen in today's climate about once every decade. However, when we consider the effect of El Niño, we find that these droughts are twice as likely to occur in El Niño years. Thus El Nino is a key driver of the 2024 event.
- To analyse the role of human-induced climate change we first looked at the relationship between global warming and rainfall anomalies in observation-based data products. We find that as global temperatures increase, rainfall in DJF also increases. This means that in the current climate, with 1.2ºC warming, droughts such as this one are actually less likely than in a cooler, pre-industrial climate. This finding is consistent with previous studies that show wetter conditions in DJF that contrast with drying in the region earlier in the season, between the months of September and November).
- To further evaluate the role of climate change in the current drought we combined the observations with climate models. The models that passed the model evaluation do not show a significant relationship between rainfall and global warming levels with increasing global temperatures.
- The analysis also indicates that with further global warming of up to 2ºC there will be no significant change in the likelihood of low rainfall in DJF as observed in the region in early 2024.
- Repeating all the analysis for the effective precipitation, taking evapotranspiration into account and only looking at water that is actually available for plants, we find very similar results.
- In summary, our analyses show that El Nino significantly increases the likelihood of such a drought to occur, while climate change did not emerge as the significant driver influencing assessed drought in the affected countries.
- As El Nino events will continue to occur in a warming climate it is important to increase resilience to droughts that will continue to occur frequently.
- Countries in the region have varying levels of development, infrastructure, and governance systems that impact their ability to respond to the drought. For example Botswana is relatively more developed than the other countries in the study and its economy and people are less reliant on rain-fed agriculture, resulting in fewer impacts.
- Maintaining robust traditional land governance systems with appropriate integration into modern frameworks appears crucial for sustainable land management and reducing drought vulnerability to southern Africa.
- Effective early warning systems, anticipatory action, and coordinated emergency response efforts are in place, and could be further strengthened by commitments for shock responsive social protection systems.

1 Introduction

From January 2024, large parts of Southern Africa experienced significantly below average precipitation. In particular, in February parts of Zimbabwe, Zambia, Malawi, Angola, Mozambique and Botswana received less than 20 percent of the typical rainfall expected for February (OCHA, 2024). As a result, most of Zimbabwe and Zambia, as well as parts of Botswana and Angola experienced their driest February on record (since 1981), while for most of Malawi and Mozambique it ranked in the top 3 (OCHA, 2024). The rainfall deficits coincided with a crucial phase of crop development in which they are especially sensitive to water stress, and is therefore expected to impact harvests later in the year (OCHA, 2024). In the same month of February, the Botswana Meteorological Services issued several (3) heatwave warnings indicating the severity of the situation, as there was not only rainfall deficit but extreme temperatures as well (BDMS, 2024). Zimbabwe has already declared a state of disaster, describing the 2023/24 cropping season as a failure due to El-Nino (PBS, 2024). Botswana is yet to declare the current cropping year a drought, but if she does, given that the 2023-23 cropping season was declared a severe agricultural drought (GOB, 2023), the impact for food security in the country could be substantial.

The bulk of Southern Africa has an austral summer rainfall regime, with the main rain-bearing systems following the south-ward movement of the Inter-Tropical Convergence Zone (ITCZ), and seasonal shifts in the positioning of the semi-permanent anticyclonic systems in the South Atlantic and South Indian ocean basins (see Figure. A1 in the appendix, Reason, 2017). Precipitation in the summer rainfall region is mostly convective, driven by large-scale tropical systems (easterly waves and remnants of tropical cyclones), to a less extent mid-latitude weather systems (cold fronts and cut-off lows), the interaction between tropical and mid-latitude systems (Tropical Temperate Troughs and Mesoscale Convective Complexes), as well as local circulations forced by variations in local topography, diurnal heating and moisture convergence associated with synoptic forcing (Rouault, et al., 2024; Reason, 2017). The presence of the Botswana high at mid-levels during the austral summer months, its strength and positioning has been shown to influence precipitation as well as frequency of dry spells in some parts of the region (Driver and Reason, 2017; Maoyi and Abiodun, 2022). The wettest months over most parts of the summer-rainfall region are December and January (Rouault, et al., 2024), with the eastern parts of the subcontinent being much wetter than the western parts (Reason, 2017). Tropical Southern-Africa tends to be wetter in the January-to-March (JFM) months when compared to the October-to-December (OND) as the ITCZ reaches its southernmost extent (Reason, 2017).

Positive states of the El Nino Southern Oscillation (i.e. El Nino conditions) are often associated with drier conditions in southern Africa due to a combination of lower rainfall and higher temperatures (Meque & Abiodun, 2014; Manatsa et al., 2017). The strength of the influence of ENSO on rainfall deficits has likely increased since the 1970s (Rouault & Richard, 2005). ENSO affects southern African weather through its influences upon the Walker circulation, Angola low and other synoptic-scale atmospheric features during the Austral summer (Hoell et al., 2015). However, the influence of this mode of variability is non-linear (Yuan et al., 2014; Gore et al., 2020; Chikoore & Jury, 2021). Different 'flavours' of ENSO event – different patterns of SST anomalies in the tropical Pacific – as well as interactions with other modes of variability such as the Indian Ocean Dipole (IOD) result in different weather patterns over southern Africa (Hoell et al., 2015; Gore et al., 2020).

To date, increases in droughts in both precipitation alone and from a combination of precipitation and temperatures have been observed in southern Africa (Spinoni et al., 2019; Dunn et al., 2020). Projections show an expected increase in intensity with further warming, due in part to an expected

shortening of the rainy season (Shongwe et al., 2009) and increase in temperatures (Spinoni et al., 2020). In accordance with these changes at the regional scale, IPCC, 2021 concluded that there has been an increase in meteorological and agricultural and ecological droughts in both eastern and western Southern Africa (Allan et al., 2023; Seneviratne et al., 2021). Evidence remains limited on the human influence on this signal. Furthermore, it projects further increases in drought in both regions with further warming, with higher magnitudes at higher warming levels (Seneviratne et al., 2021).

Prior attribution studies give estimates of changing drought hazards for regional and subregional spatial scales, and from months to multi-year events. A study on the very dry December-February period of 2002/03, considering all land regions below 10S on the African continent and Madagascar, found that such dry summers had become about 40% more likely due to anthropogenic climate change (Bellprat et al., 2015). For a region over most of Zimbabwe, central Mozambique, northern South Africa and southern Zambia, the precipitation in December-February of 2015/16 was reduced by around 24% due to the influence of anthropogenic climate change on El Nino SSTs, with an additional small effect due to local air temperatures (Funk et al., 2016). The December-January 2015/16 'flash drought' in southern Africa, assessed as all land regions below 10S on the African continent (but not Madagascar), was found to have more than tripled in likelihood due to anthropogenic climate change (Yuan et al., 2018). Several studies have assessed anthropogenic influences on the western Cape drought in South Africa. Considered over the period 2015-19, this drought was made twice as likely to occur (Kam et al., 2021), while from 2015-17 it was made from 3-6 times as likely (Otto et al., 2018; Pascale et al., 2020). The message from previous studies is consistent in projecting an increasing likelihood and intensity of drought. However, these studies are all multi-year events in a small region in South Africa, or December-February (DJF) periods over the entire southern Africa region or a specific subregion in eastern Southern Africa. The event under study here is most closely characterised by the DJF period over eastern southern Africa, assessed by Funk et al. (2016), but covers much larger parts of Botswana and Zambia in particular, and doesn't incorporate South Africa.

1.2 Event Definition

The year 2023 was confirmed as the warmest on record, with the global average near-surface temperature reaching 1.45 °Celsius (WMO, 2023). El Niño conditions experienced in 2023 were considered as one of the five strongest on record, in terms of absolute Niño 3.4 values. Strong El Niño conditions coupled with climate change fuel record temperatures and extreme events (Santoso, et al., 2017) especially in the tropics (Rifai et al., 2019) . In this study, we assess the relative role of anthropogenic climate and El Niño in the severity of drought that resulted in devastating impacts in southern Africa. For event definition (both spatial and temporal) two things are important: the relation to the impact of the event, and the climatological homogeneity of the area. We select a spatially and climatologically homogeneous region (blue outline in figure 1) encompassing Botswana, Zimbabwe, southern Zambia and southern Mozambique, with a cut off over Zambia and Mozambique at a boundary in the north at 16S. We assess basic precipitation deficit and the influence of temperature on drought through evapotranspiration in relation to precipitation. We analyse December-January-February (DJF) total rainfall and total effective precipitation. Effective precipitation is the difference between total rainfall and Potential Evapotranspiration (PET). PET is estimated using the Hargreaves-Samani method (Hargreaves & Samani, 1985). Figure 1 (a) shows the rainfall anomaly in the total DJF rainfall with respect to 1980-2023 climatology. To characterise the drought event, we employ Standardised Precipitation Evapotranspiration Index (SPEI) obtained over the 3-month period (December 2023 to

February 2024), spanning the entire Southern Africa region. The colour scheme reflects the US Drought Monitor drought classifications (D0 - abnormally dry, D1 - moderate, D2 - severe, D3 - extreme, and D4 - exceptional). SPEI (climatic water balance) is calculated using effective rainfall and PET. Both meteorological drought (a) and agricultural drought (b) range from severe to exceptional across the study area, particularly the western and northern regions. Figure 2 and 3 show the evolution of total rainfall and effective rainfall, respectively, over the season from 1980-2024 in different datasets.

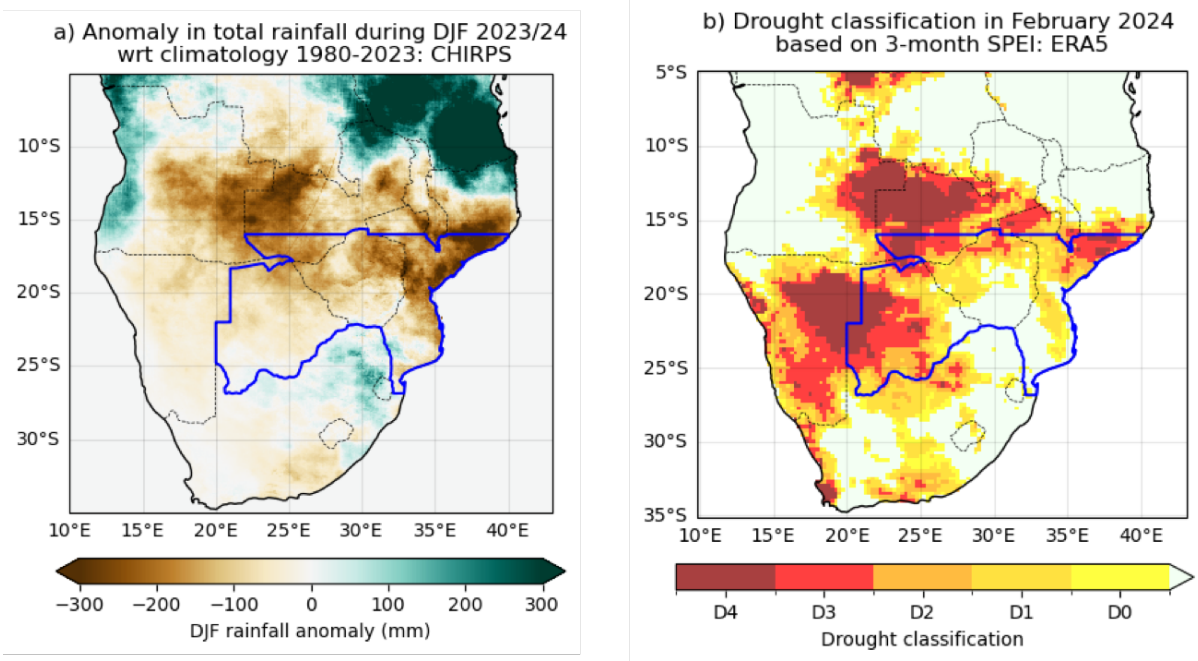

Figure 1 (a) Season rainfall anomaly *over December 2023 to February 2024 period relative to the 1980-2010 climatology in the CHIRPS dataset* ***(b) Drought classifications*** *based on Standardised Precipitation Evapotranspiration Index (SPEI), showing the magnitudes of precipitation deficit from December 2023 to February 2024 relative to the 1980-2023 climatology in the ERA5 dataset. The colour scheme reflects the US Drought Monitor drought classifications (D0 - abnormally dry, D1 - moderate, D2 - severe, D3 - extreme, and D4 - exceptional). The bold blue outline highlights the study region.*

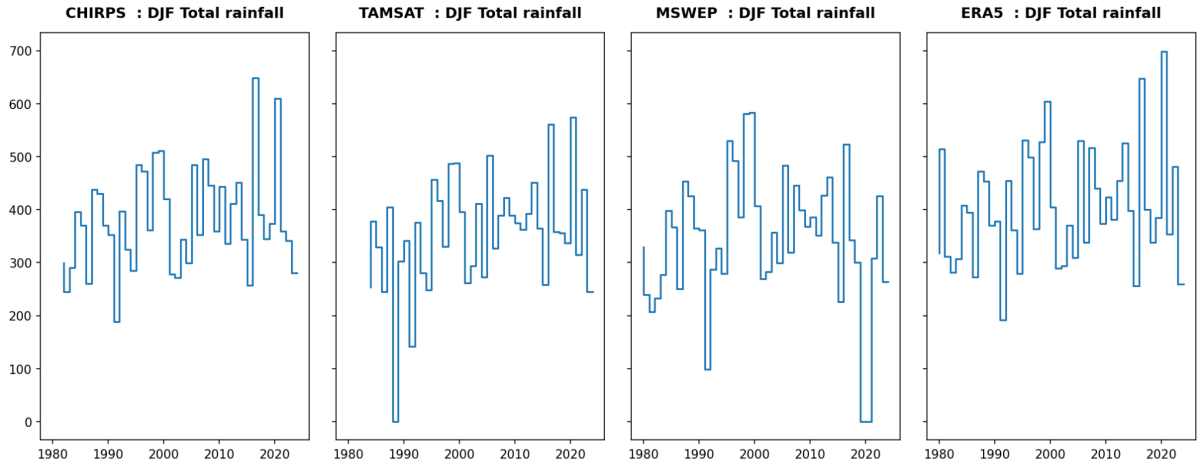

Figure 2. ***Total seasonal*** *rainfall over December-January-February for the period 1980-2024 over the study region in CHIRPS (a) , TAMSAT (b), MSWEP (c), and ERA5 (d) datasets.*

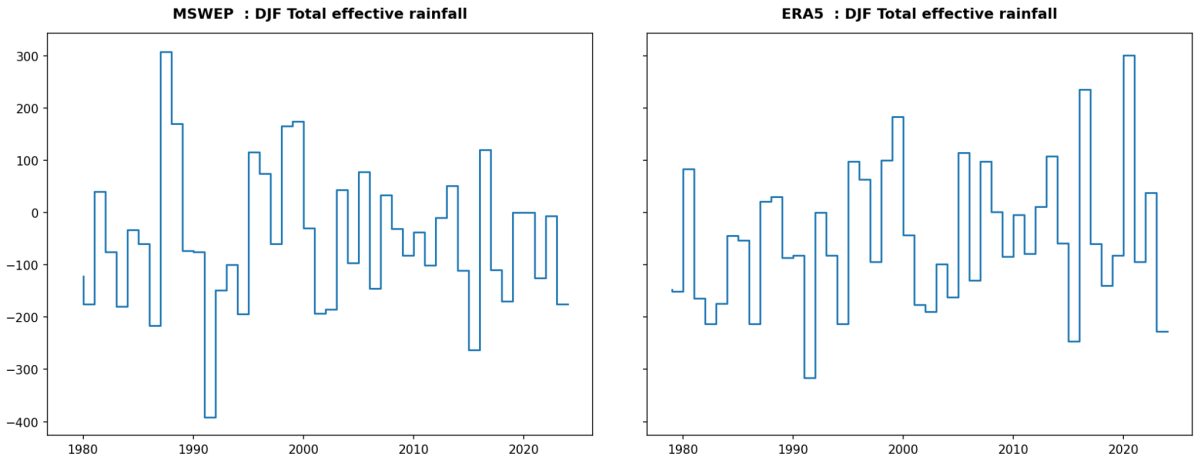

Figure 3. ***Total seasonal*** *accumulation of effective rainfall over December-January-February for the period 1980-2024 over the study region in MSWEP/MSWX and ERA5 datasets.*

2 Data and methods

2.1 Observational data

2.1.1. Gridded products

We use daily data for four gridded observational datasets:

(i) Climate Hazards Group InfraRed Precipitation with Station data (CHIRPS). CHIRPS (Climate Hazards Group InfraRed Precipitation with Station data; Funk et al., 2015b). CHIRPS is the state of the art observational daily dataset developed by the UC Santa Barbara Climate Hazards Group called "Climate Hazards Group InfraRed Precipitation with Station data" available for the period 1981–present. For this dataset, we utilised daily rainfall data from 1981-2024.

(ii) Tropical Applications of Meteorology using SATellite and ground based observations (TAMSAT). TAMSAT is a daily rainfall dataset based on high-resolution thermal-infrared observations generated by breaking down 5-day total TAMSAT rainfall estimates into daily increments, achieved through the utilisation of daily cold cloud duration information. We used the daily rainfall dataset available from 1983 to the present.

(iii) Multi-Source Weather (MSWX) and Multi-Source Weighted-Ensemble Precipitation (MSWEP). MSWX and MSWEP is an operational, high-resolution, bias-corrected (based on ERA5 data bias-corrected and downscaled using high-resolution reference climatologies) meteorological product with global coverage from 1979 to 7 months from now. These products combine gauge-, satellite-, and reanalysis-based data for reliable precipitation estimates, at 3-hourly intervals from 1979 to near real-time, and at 0.1° spatial resolution globally. The two products are designed to be fully compatible (Beck et al., 2022). For this analysis, we use precipitation from MSWEP and minimum and maximum temperatures from MSWX.

(iv) ERA5 (5th Generation product from the European Centre for Medium-Range Weather Forecasts (ECMWF). ERA5 reanalysis product begins in the year 1950 (Hersbach et al., 2020). We use monthly rainfall, maximum and minimum temperature from this product. It should be noted that the variables from ERA5 are not directly assimilated, but these are generated by atmospheric components of the Integrated Forecast System (IFS) modelling system. For this product, we utilised only data from 1979

onwards from both datasets due its low performance in the pre-satellite period. All datasets were used to define the event, evaluate the models and conduct attribution analysis.

2.1.2. Observed global mean surface temperature

As a measure of anthropogenic climate change, we use the (low-pass filtered) global mean surface temperature (GMST), where GMST is taken from the National Aeronautics and Space Administration (NASA) Goddard Institute for Space Science (GISS) surface temperature analysis (GISTEMP, Hansen et al., 2010 and Lenssen et al. 2019).

2.1.3. El Niño Index

As a measure of the El Niño - Southern Oscillation cycle (ENSO) we use the relative Nino3.4 index as defined in Van Oldenborgh et al., 2021. This is the Nino3.4 index (average SST over 5° S–5° N, 120°–170° W) minus the SST between 20° S–20° N to adjust the index for climate change. Because we are averaging the index over a period of several months, the values are not standardised per calendar month.

2.2 Model and experiment descriptions

We use two multi-model ensembles from climate modelling experiments using different framings (Philip et al., 2020): Regional climate models and coupled global circulation models.

1. Coordinated Regional Climate Downscaling Experiment (CORDEX)-Africa Domain (AFR-CORDEX) with 0.44° resolution (Giorgi et al. 2009) comprising 11 simulations resulting from pairings of Global Climate Models (GCMs) and Regional Climate Models (RCMs). These simulations are composed of historical simulations from 1950 up to 2005, and extended to the year 2100 using the RCP8.5 scenario.

2. Coupled Model Intercomparison Project Phase 6 (CMIP6), which consists of simulations from 20 participating models with varying resolutions. For more details on CMIP6, please see Eyring et al., (2016). For all simulations, the period 1850 to 2015 is based on historical simulations, while the SSP5-8.5 scenario is used for the remainder of the 21st century.

2.3 Statistical methods

In this study, we analyse time series of precipitation and effective precipitation, area averaged over the study region in southern Africa (shown in Fig. 1), using observational datasets and climate model simulations. Methods for observational and model analysis and for model evaluation and synthesis are used according to the World Weather Attribution Protocol, described in Philip et al. (2020), with supporting details found in van Oldenborgh et al. (2021), Ciavarella et al. (2021) and here. The analysis steps include: (i) trend calculation from observations; (ii) model evaluation; (iii) multi-method multi-model attribution and (iv) synthesis of the attribution statement. We calculate the return periods, Probability Ratio (PR; the factor-change in the event's probability) and change in intensity of the event under study in order to compare the climate of now and the climate of the past, defined respectively by the GMST values of now and of the preindustrial past (1850-1900, based on the Global Warming Index). To statistically model the event under study, we use Gaussian distribution for both precipitation (the distribution scaled with GMST) and for effective precipitation (distribution shifted with GMST).

To account for potential changes in drought conditions due to regional warming and teleconnection patterns, we supplement the standard WWA protocol by assessing the relative role of climate change El Niño state of DJF 2023/2024.

2.3.1 Supplementary methods

In order to understand the contribution of the strong 2023/2024 El Niño event on the drought, we supplement this analysis with a model that uses both GMST and the detrended Niño3.4 index as covariates, as described below. In this model, the covariate used is the mean of the detrended Niño3.4 index from December- February; in other words, the detrended Niño3.4 index averaged over the same period that the precipitation and effective precipitation are accumulated over.

Analysis of drivers of changing rainfall deficit and effective rainfall

(i) The variable of interest, X, is assumed to follow a normal distribution in which the location parameter varies with both GMST and the detrended Niño3.4 index, while the variance of the distribution is remains constant, so that

$$X \sim N(\mu, \sigma \mid \mu_0, \alpha, \beta, T, N), \text{ where } \mu = \mu_0 + \alpha T + \beta N$$

where X denotes the variable of interest, DJF rainfall or DJF effective rainfall; T is the smoothed GMST, N is the detrended DJF Niño3.4 index, μ and σ are the mean and variance parameters of the non-stationary distribution and α, β are the trends due to GMST and Niño3.4, respectively. As a result, the location of the distribution has a different value in each year, determined by both the GMST and Niño3.4. Maximum likelihood estimation is used to estimate the model parameters

(ii) We fit Gaussian distributions that scale with GMST to the observed DJF accumulated precipitation (X) time series:

$$X \sim N(\mu_X, \sigma_X \mid \mu_{0X}, \alpha_X, \beta_X, T, N)$$

(iii) We fit Gaussian distributions that shifts with GMST to the observed DJF accumulated effective precipitation (Y) time series respectively:

$$Y \sim N(\mu_Y, \sigma_Y, \alpha_Y, \beta_Y, T, N)$$

(iv) We use the cumulative distribution functions (CDFs) of these two distributions to compute the probabilities u and v of exceeding the values observed at each time t, so that

$$u_t = P(X \leq x_t) \quad \text{and} \quad v_t = 1 - P(Y \leq y_t)$$

Note that, because we are interested in the lower tails of the precipitation distribution and the upper tails of the effective precipitation distribution, these exceedance probabilities are given by the CDF of X and (1 - the CDF of Y).

3 Observational analysis: return period and trend

3.1 Analysis of gridded data

Figures. 4(a-d) shows the results from the trend-fitting methods applied to the DJF total rainfall in the study region, from CHIRPS, TAMSAT, MSWEP and ERA5, respectively, for the period 1980/81-2023/24. Figures. 4a(i)-d(i) show the variable as a function of the GMST anomaly only while figures 4a(ii)-d(ii) show the variable as a function of both GMST and DJF detrended 3.4 Nino anomalies. All datasets show an increasing trend in the DJF total rainfall in this region due to changes in GMST and a decreasing trend due to combined effect of GMST and strong El Niño conditions of 2023. Table 1 presents return periods of the DJF low rainfall event as a result of GMST and Nino influence and for GMST only. Under both GMST and Nino influence, the 2023/24 event becomes more common compared to under GMST influence only. For the former, a return period of 4 years (uncertainty: 2 to 13 years) is seen in CHIRPS; 21 years (uncertainty: 8 to 87 years) in TAMSAT; 21 years (uncertainty: 8 to 87 years) in MSWEP; and 21 years (uncertainty: 8 to 87 years) in ERA5. For the later i.e GMST-only influence, a return period of 12 years (uncertainty: 5 to 41 years) is shown in CHIRPS; 10 years (uncertainty: 4 to 62 years) in TAMSAT; 4 years (uncertainty: 2 to 10 years) in MSWEP; and 19 years (uncertainty: 8 to 66 years) in ERA5. This suggests that under GMST-only changes, droughts such as this one are expected to happen in today's climate about once every decade. However, when we consider the effect of El Niño, these droughts become twice as likely to occur in El Niño years. For the model analysis we use a return period of 10 years.

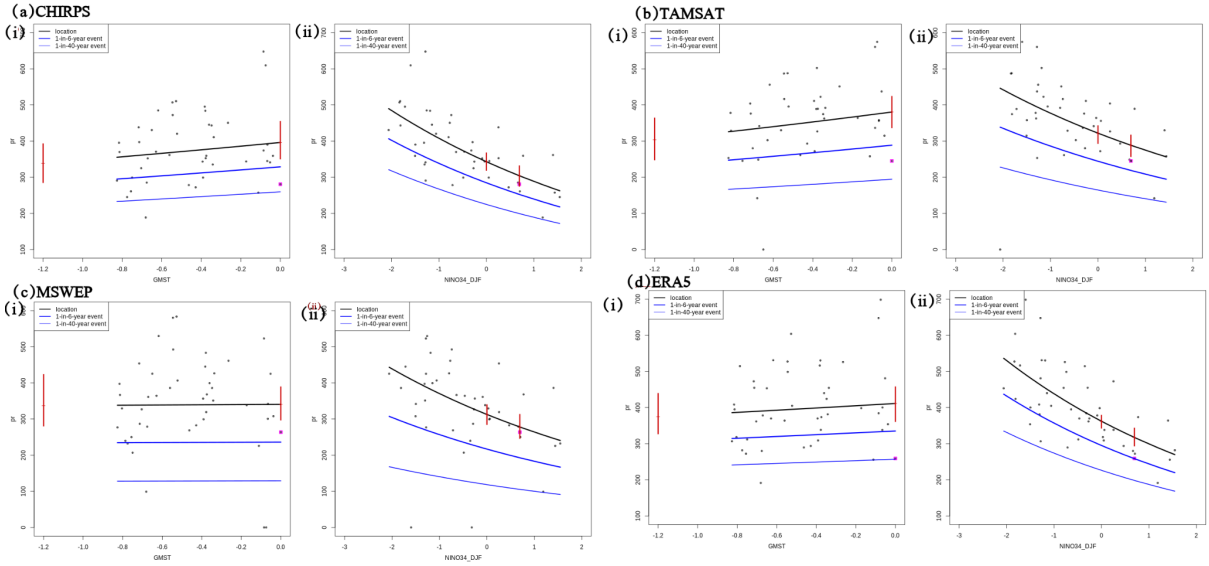

***Figure 4. (a) DJF total rainfall** over the study region estimated from CHIRPS dataset shown against the change in **global mean temperature only (i)** and change in **both global mean temperature and DJF detrended 3.4 Niño (ii)**. The thick red line denotes the time-varying mean. The vertical red lines show the 95% confidence interval for the location parameter, for the current, 2023/24 climate and the hypothetical, 1.2℃ cooler climate. The 2023/24 observation is highlighted with the red box. The black line indicates the location of the fitted distribution, and the blue lines indicate estimated 6- and 40-year return levels. **(b) , (c) , (d)** are the same as (a), based on TAMSAT, MSWEP and ERA5 datasets, respectively.*

***Table 1. Return periods** in DJF rainfall over the study region in 2023/2024 due to combined influence of El Niño conditions and GMST, and influence from GMST only. In brackets are 2.5 and 97.5% confidence intervals, respectively*

	Return periods conditioned on both Niño and GMST	Return periods conditioned on on GMST only
CHIRPS	4.3 (2.1 - 13.7)	12.4 (5.9 - 41.4)
TAMSAT	5.1(2.7 - 26.3)	10.8 (4.8 - 62.2)
MSWEP	2.3 (1.5 - 4.8)	4.0 (2.4 - 10.5)
ERA5	7.4 (3.3 - 26.7)	19.5 (8.9 - 66.2)

Figures. 5(a-b) shows the results from the trend-fitting methods applied to the DJF total effective rainfall in the study region, from ERA5 and MSWX/MSWEP respectively, for the period 1980/81-2023/24. Figures 5a(i)-b(i) show the variable as a function of the GMST anomaly only while figures 4a(ii)-b(ii) show the variable as a function of both GMST and DJF detrended Niño 3.4 anomalies. Same as rainfall, increasing trends are seen as GMST increases but combined effect of EL Niño conditions show that effective rainfall in this region is decreasing. Similarly, these trends also suggest a likely doubling to tripling of the chances of similar events with effect on El Niño (Table 2; 5 and 2 years under both GMST and El Niño and 24 and 5 years under GMST only, for ERA5 and MSWX/MSWEP respectively). For the model analysis we use a return period of 10 years

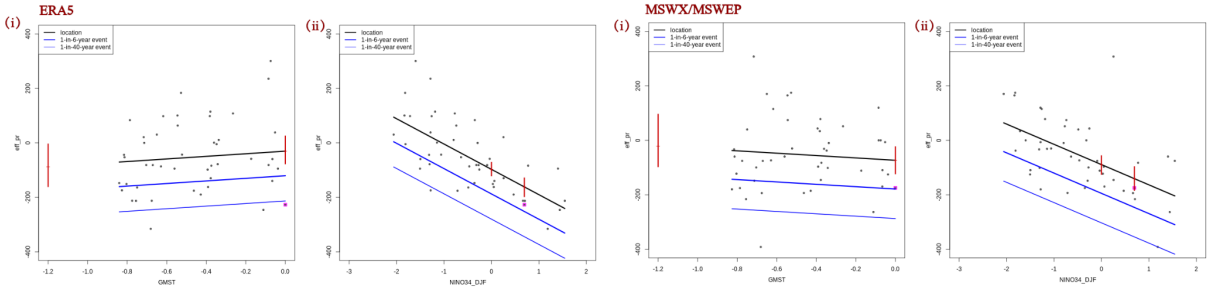

Figure 5. (a) DJF total effective rainfall *over the study region estimated from ERA5 dataset shown against the change in* ***global mean temperature only (i)*** *and change in* ***both global mean temperature and DJF detrended 3.4 Niño (ii)****. The thick red line denotes the time-varying mean. The vertical red lines show the 95% confidence interval for the location parameter, for the current, 2023/24 climate and the hypothetical, 1.2ºC cooler climate. The 2023/24 observation is highlighted with the red box. The black line indicates the location of the fitted distribution, and the blue lines indicate estimated 6- and 40-year return levels.* ***(b)*** *is the same as (a), but based on MSWX/MSWEP datasets.*

Table 2. *Return periods in DJF effective rainfall over the study region in 2023/2024 due to combined influence of El Niño conditions and GMST, and influence from GMST only. In brackets are 2.5 and 97.5% confidence intervals, respectively*

	Return periods conditioned on both Niño and GMST	Return periods conditioned on GMST only
ERA5	5.7 (2.8 - 25.0)	24.8 (8.2 - 151.6)
MSWX/MSWEP	2.2 (1.5 - 4.5)	5.6 (3.1 - 16.4)

In general, the observational analysis reveals that the drought conditions experienced in southern Africa during 2023/2024 DJF were likely significantly influenced by the strong 2023 El Niño event, which began early in the year and persisted throughout. We explored this by our statistical model to integrate the detrended Niño3.4 index (as outlined in Section 2.1) as an additional covariate, as elaborated in Section 2.3.1. Our findings indicate that the likelihood of such droughts occurring doubles or even triples during El Niño years. Consequently, El Niño emerges as a primary driver for the 2023/2024 drought event in southern Africa.

4 Model evaluation

In Table 1 below we show the results of the model evaluation for the southern Africa region, for DJF precipitation. The climate models are evaluated against the observations in their ability to capture the seasonal cycle and spatial pattern using the CHIRPS and TAMSAT datasets as a reference. Models are also evaluated in terms of how well the statistical distribution of rainfall matches that of the observational datasets: if the best estimate of the scale parameter falls within the range of values estimated from the observations, the model is deemed 'good'; if the estimated confidence intervals overlap, the model is 'reasonable'; and if the confidence intervals do not overlap, the model is 'bad'. We rate the model as overall 'reasonable' or 'bad', if it is rated 'reasonable' or 'bad', respectively, for at least one criterion. If more than five models are rated 'good' for any framing, we use only the 'good' models in the attribution; otherwise we also include 'reasonable' models. We do not evaluate the models for the effective precipitation. We choose those models that pass the evaluation for precipitation for effective precipitation attribution analysis. Per framing or model setup we also use models that only just pass the evaluation tests if we only have five models or less for that framing that perform well.

***Table 4**: **Evaluation results** of the climate models considered for attribution analysis of DJF precipitation over the study region. For each model, the expected values of a 1-in-10 -year event is shown, along with the best estimate of the dispersion and the 95% confidence interval obtained via bootstrapping. Based on overall suitability, the models are classified as good, reasonable or bad, shown by green, yellow and red highlights, respectively.*

Model / Observations	**Seasonal cycle**	**Spatial pattern**	**Dispersion**	**Event magnitude (mm)**
CHIRPS			0.241 (0.188 ... 0.275)	280.717
TAMSAT			0.288 (0.196 ... 0.381)	245.048
ERA5			0.258 (0.201 ... 0.295)	258.979
MSWEP			0.361 (0.246 ... 0.474)	263.781
				Magnitude of 10-year event (mm)
CMIP6				
ACCESS-CM2 historical-ssp585 (1)	reasonable	reasonable	0.220 (0.177 ... 0.253)	422.681
ACCESS-ESM1-5 historical-ssp585 (1)	reasonable	good	0.185 (0.140 ... 0.216)	475.504
CanESM5 historical-ssp585 (1)	good	reasonable	0.189 (0.143 ... 0.230)	554.049
CMCC-ESM2 historical-ssp585 (1)	good	reasonable	0.142 (0.104 ... 0.178)	517.847
CNRM-CM6-1-HR historical-ssp585 (1)	good	good	0.269 (0.217 ... 0.304)	194.752
CNRM-CM6-1 historical-ssp585 (1)	good	good	0.198 (0.157 ... 0.234)	259.520

EC-Earth3-Veg-LR historical-ssp585 (1)	bad	reasonable	0.136 (0.111 ... 0.156)	505.002
EC-Earth3-Veg historical-ssp585 (1)	reasonable	reasonable	0.178 (0.131 ... 0.217)	448.016
EC-Earth3 historical-ssp585 (1)	reasonable	good	0.186 (0.146 ... 0.218)	417.994
FGOALS-g3 historical-ssp585 (1)	reasonable	good	0.192 (0.143 ... 0.220)	243.825
INM-CM4-8 historical-ssp585 (1)	good	good	0.242 (0.193 ... 0.277)	320.161
INM-CM5-0 historical-ssp585 (1)	good	reasonable	0.248 (0.203 ... 0.280)	332.758
IPSL-CM6A-LR historical-ssp585 (1)	reasonable	bad	0.112 (0.0886 ... 0.129)	561.911
MIROC6 historical-ssp585 (1)	reasonable	reasonable	0.176 (0.141 ... 0.206)	540.561
MPI-ESM1-2-HR historical-ssp585 (1)	good	good	0.235 (0.175 ... 0.280)	285.159
MPI-ESM1-2-LR historical-ssp585 (1)	reasonable	bad	0.180 (0.125 ... 0.216)	341.885
MRI-ESM2-0 historical-ssp585 (1)	reasonable	good	0.172 (0.126 ... 0.216)	421.150
NorESM2-LM historical-ssp585 (1)	reasonable	reasonable	0.184 (0.144 ... 0.221)	333.450
NorESM2-MM historical-ssp585 (1)	good	reasonable	0.189 (0.140 ... 0.226)	348.891
TaiESM1 historical-ssp585 (1)	reasonable	reasonable	0.140 (0.114 ... 0.159)	456.376
CORDEX ()			(...)	
CanESM2_rcp85_r1i1p1_SMHI-RCA4 historical-rcp85 (1)	good	good	0.226 (0.180 ... 0.267)	302.362
CNRM-CM5_rcp85_r1i1p1_SMHI-RCA4 historical-rcp85 (1)	good	reasonable	0.184 (0.150 ... 0.213)	366.646
CSIRO-Mk3-6-0_rcp85_r1i1p1_SMHI-RCA4 historical-rcp85 (1)	reasonable	reasonable	0.202 (0.159 ... 0.240)	288.669
EC-EARTH_rcp85_r1i1p1_KNMI-RACMO22T historical-rcp85 (1)	reasonable	reasonable	0.113 (0.0847 ... 0.134)	379.833
EC-EARTH_rcp85_r1i1p1_SMHI-RCA4 historical-rcp85 (1)	reasonable	good	0.159 (0.125 ... 0.182)	347.755
IPSL-CM5A-MR_rcp85_r1i1p1_SMHI-RCA4 historical-rcp85 (1)	reasonable	reasonable	0.219 (0.174 ... 0.254)	292.980
MIROC5_rcp85_r1i1p1_SMHI-RCA4 historical-rcp85 (1)	reasonable	good	0.172 (0.130 ... 0.200)	422.393
MPI-ESM-LR_rcp85_r1i1p1_SMHI-RCA4 historical-rcp85 (1)	reasonable	reasonable	0.210 (0.167 ... 0.240)	309.953
NorESM1-M_rcp85_r1i1p1_SMHI-RCA4 historical-rcp85 (1)	good	good	0.137 (0.111 ... 0.155)	454.762
GFDL-ESM2M_rcp85_r1i1p1_SMHI-RCA4 historical-rcp85 (1)	good	reasonable	0.172 (0.131 ... 0.208)	315.786

***Table 5**:same as Table 1, for **DJF effective precipitation**, averaged over the study region.*

Model / Observations	**Seasonal cycle**	**Spatial pattern**	**Sigma**	**Event magnitude (mm)**
ERA5			128 (100 ... 147)	-227.089
MSWX			130 (99.1 ... 159)	-174.636

				Magnitude of 10-year event(mm)
CMIP6				
ACCESS-CM2 historical-ssp585 (1)	reasonable	reasonable	190 (141 ... 226)	54.50
ACCESS-ESM1-5 historical-ssp585 (1)	reasonable	good	209 (166 ... 235)	112.88
CanESM5 historical-ssp585 (1)	good	reasonable	224 (168 ... 266)	577.04
CMCC-ESM2 historical-ssp585 (1)	good	reasonable	125 (97.2 ... 144)	508.43
CNRM-CM6-1-HR historical-ssp585 (1)	good	good	137 (110 ... 157)	-237.07
CNRM-CM6-1 historical-ssp585 (1)	good	good	127 (104 ... 146)	-147.97
EC-Earth3-Veg-LR historical-ssp585 (1)	bad	reasonable	136 (108 ... 158)	135.00
EC-Earth3-Veg historical-ssp585 (1)	reasonable	reasonable	149 (118 ... 176)	84.80
EC-Earth3 historical-ssp585 (1)	reasonable	good	162 (123 ... 190)	50.10
FGOALS-g3 historical-ssp585 (1)	reasonable	good	106 (84.5 ... 121)	267.10
INM-CM4-8 historical-ssp585 (1)	good	good	155 (122 ... 175)	309.80
INM-CM5-0 historical-ssp585 (1)	good	reasonable	179 (147 ... 200)	337.36
IPSL-CM6A-LR historical-ssp585 (1)	reasonable	bad	106 (81.1 ... 122)	217.33
MIROC6 historical-ssp585 (1)	reasonable	reasonable	197 (160 ... 229)	7.50
MPI-ESM1-2-HR historical-ssp585 (1)	good	good	146 (110 ... 175)	-169.20
MPI-ESM1-2-LR historical-ssp585 (1)	reasonable	bad	119 (91.7 ... 138)	-60.35
MRI-ESM2-0 historical-ssp585 (1)	reasonable	good	125 (94.7 ... 149)	-69.00
NorESM2-LM historical-ssp585 (1)	reasonable	reasonable	95.0 (73.4 ... 110)	360.38
NorESM2-MM historical-ssp585 (1)	good	reasonable	125 (98.9 ... 144)	394.65
CORDEX				
CanESM2_rcp85_r1i1p1_SMHI-RCA4 historical-rcp85 (1)	good	good	138 (105 ... 160)	263.26
CNRM-CM5_rcp85_r1i1p1_SMHI-RCA4 historical-rcp85 (1)	good	reasonable	137 (109 ... 161)	-47.93
CSIRO-Mk3-6-0_rcp85_r1i1p1_SMHI-RCA4 historical-rcp85 (1)	reasonable	reasonable	133 (99.7 ... 166)	247.17
EC-EARTH_rcp85_r1i1p1_KNMI-RACMO22T historical-rcp85 (1)	reasonable	reasonable	83.1 (64.9 ... 94.5)	-47.94
EC-EARTH_rcp85_r1i1p1_SMHI-RCA4 historical-rcp85 (1)	reasonable	good	123 (94.5 ... 143)	-114.31
IPSL-CM5A-MR_rcp85_r1i1p1_SMHI-RCA4 historical-rcp85 (1)	reasonable	reasonable	144 (116 ... 164)	355.98
MIROC5_rcp85_r1i1p1_SMHI-RCA4 historical-rcp85 (1)	reasonable	good	158 (121 ... 185)	364.69
MPI-ESM-LR_rcp85_r1i1p1_SMHI-RCA4 historical-rcp85 (1)	reasonable	reasonable	173 (136 ... 200)	-121.85
NorESM1-M_rcp85_r1i1p1_SMHI-RCA4 historical-rcp85 (1)	good	good	154 (117 ... 181)	445.69
GFDL-ESM2M_rcp85_r1i1p1_SMHI-RCA4 historical-rcp85 (1)	good	reasonable	115 (91.5 ... 133)	283.01

5 Multi-method multi-model attribution

This section shows Probability Ratios and change in intensity ΔI for models that passed the evaluation tests and also includes the values calculated from the fits with observations.

***Table 6**: **Probability ratio and change in intensity** of an event such as the recent 2023/24 DJF precipitation due to changing GMST, for the study region: (a) from pre industrial climate to the present and (b) from the present to 2C above preindustrial.*

	a. Past vs. present		b. Present vs. future	
Model / Observations	**Probability ratio PR [-]**	**Change in intensity ΔI [%]**	**Probability ratio PR [-]**	**Change in intensity ΔI [%]**
CHIRPS	0.24 (0.047 ... 1.8)	35 (-11 ... 89)		
TAMSAT	0.29 (0.051 ... 1.4)	39 (-4.7 ... 97)		
MSWEP	0.89 (0.23 ... 2.6)	4.7 (-30 ... 58)		
ACCESS-CM2 historical-ssp585 (1)	1.1 (0.60 ... 2.1)	-1.1 (-10 ... 7.7)	0.95 (0.77 ... 1.2)	0.79 (-2.3 ... 3.8)
ACCESS-ESM1-5 historical-ssp585 (1)	4.5 (2.3 ... 10)	-16 (-23 ... -8.6)	1.2 (0.94 ... 1.6)	-2.4 (-6.1 ... 0.76)
CanESM5 historical-ssp585 (1)	1.2 (0.76 ... 1.9)	-2.4 (-8.1 ... 3.6)	1.1 (0.93 ... 1.3)	-1.0 (-3.2 ... 0.92)
CNRM-CM6-1-HR historical-ssp585 (1)	1.1 (0.63 ... 1.9)	-1.4 (-13 ... 10)	1.2 (1.0 ... 1.4)	-4.5 (-9.4 ... -0.049)
CNRM-CM6-1 historical-ssp585 (1)	1.4 (0.82 ... 2.5)	-5.0 (-14 ... 3.2)	1.3 (1.0 ... 1.6)	-4.6 (-9.4 ... -0.69)
EC-Earth3-Veg historical-ssp585 (1)	1.0 (0.62 ... 1.7)	-0.26 (-6.9 ... 6.0)	0.88 (0.73 ... 1.1)	1.5 (-0.64 ... 3.6)
EC-Earth3 historical-ssp585 (1)	1.4 (0.84 ... 2.4)	-4.2 (-11 ... 2.0)	0.87 (0.67 ... 1.1)	1.7 (-1.7 ... 4.6)
FGOALS-g3 historical-ssp585 (1)	1.0 (0.59 ... 1.7)	0.00025 (-7.1 ... 7.2)	1.1 (0.90 ... 1.4)	-1.6 (-5.3 ... 1.4)
INM-CM4-8 historical-ssp585 (1)	0.67 (0.35 ... 1.4)	8.4 (-6.7 ... 22)	1.0 (0.72 ... 1.3)	0.041 (-5.8 ... 5.9)
INM-CM5-0 historical-ssp585 (1)	1.1 (0.62 ... 2.1)	-1.8 (-16 ... 12)	0.77 (0.64 ... 0.95)	6.2 (1.3 ... 10)
MIROC6 historical-ssp585 (1)	1.0 (0.43 ... 3.1)	-0.013 (-12 ... 10)	0.84 (0.57 ... 1.1)	1.9 (-1.1 ... 5.8)
MPI-ESM1-2-HR historical-ssp585 (1)	0.92 (0.49 ... 2.0)	1.5 (-11 ... 13)	1.2 (0.98 ... 1.6)	-4.1 (-8.3 ... 0.35)
MRI-ESM2-0 historical-ssp585 (1)	1.3 (0.70 ... 2.4)	-3.4 (-11 ... 4.6)	1.3 (1.0 ... 1.6)	-3.2 (-6.4 ... -0.18)
NorESM2-LM historical-ssp585 (1)	3.4 (1.6 ... 9.6)	-16 (-26 ... -6.1)	1.5 (1.1 ... 2.1)	-6.5 (-12 ... -1.9)
NorESM2-MM historical-ssp585 (1)	1.7 (0.80 ... 4.3)	-6.8 (-17 ... 3.2)	1.2 (0.95 ... 1.7)	-3.0 (-7.5 ... 0.72)
CanESM2_rcp85_r1i1p1_SMHI-RCA4 historical-rcp85 (1)	0.56 (0.26 ... 1.0)	11 (-0.68 ... 21)	0.95 (0.75 ... 1.1)	0.84 (-2.4 ... 4.4)
CNRM-CM5_rcp85_r1i1p1_SMHI-RCA4 historical-rcp85 (1)	1.2 (0.40 ... 4.6)	-2.1 (-16 ... 11)	1.1 (0.82 ... 1.6)	-1.7 (-6.0 ... 2.1)

CSIRO-Mk3-6-0_rcp85_r1i1p1_SMHI-RCA4 historical-rcp85 (1)	0.89 (0.31 ... 3.0)	2.2 (-18 ... 22)	0.95 (0.68 ... 1.3)	1.0 (-5.0 ... 6.6)
IPSL-CM5A-MR_rcp85_r1i1p1_SMHI-RCA4 historical-rcp85 (1)	0.70 (0.29 ... 1.9)	6.3 (-11 ... 20)	0.99 (0.74 ... 1.2)	0.15 (-4.3 ... 4.9)
MIROC5_rcp85_r1i1p1_SMHI-RCA4 historical-rcp85 (1)	0.94 (0.34 ... 4.0)	0.83 (-15 ... 15)	1.4 (0.97 ... 1.9)	-4.4 (-9.5 ... 0.35)
MPI-ESM-LR_rcp85_r1i1p1_SMHI-RCA4 historical-rcp85 (1)	1.5 (0.66 ... 3.6)	-6.5 (-18 ... 6.8)	1.2 (0.95 ... 1.6)	-2.8 (-6.8 ... 0.61)
GFDL-ESM2M_rcp85_r1i1p1_SMHI-RCA4 historical-rcp85 (1)	5.3 (1.3 ... 31)	-17 (-28 ... -2.8)	1.1 (0.74 ... 1.7)	-1.3 (-5.5 ... 2.7)

***Table** 7: Probability ratio and change in intensity of an event such as the recent 2023/24 DJF effective precipitation due to changing GMST, for the study region: (a) from pre industrial climate to the present and (b) from the present to 2C above preindustrial.*

Model / Observations	**a. Past vs. present**		**b. Present vs. future**	
	Probability ratio PR [-]	**Change in intensity ΔI [mm]**	**Probability ratio PR [-]**	**Change in intensity ΔI [mm]**
ERA5	0.18 (0.016 ... 2.4)	1.2e+2 (-51 ... 2.7e+2)		
MSWX	1.0 (0.17 ... 11)	-0.20 (-1.7e+2 ... 1.5e+2)		
ACCESS-CM2 historical-ssp585 (1)	1.4 (0.55 ... 3.1)	-35 (-1.2e+2 ... 51)	0.95 (0.60 ... 1.3)	5.1 (-27 ... 42)
CMCC-ESM2 historical-ssp585 (1)	1.8 (0.92 ... 3.6)	-40 (-92 ... 6.2)	1.1 (0.83 ... 1.5)	-8.8 (-29 ... 12)
CNRM-CM6-1-HR historical-ssp585 (1)	1.5 (0.58 ... 3.1)	-26 (-80 ... 30)	1.5 (1.2 ... 1.8)	-33 (-55 ... -11)
CNRM-CM6-1 historical-ssp585 (1)	1.5 (0.69 ... 3.5)	-30 (-97 ... 24)	1.5 (1.2 ... 1.8)	-35 (-62 ... -13)
EC-Earth3-Veg historical-ssp585 (1)	1.0 (0.50 ... 1.7)	-0.050 (-49 ... 54)	0.84 (0.64 ... 1.1)	13 (-4.3 ... 30)
EC-Earth3 historical-ssp585 (1)	1.3 (0.62 ... 2.6)	-21 (-88 ... 38)	0.88 (0.53 ... 1.2)	11 (-20 ... 43)
FGOALS-g3 historical-ssp585 (1)	1.1 (0.49 ... 2.3)	-5.4 (-51 ... 38)	1.1 (0.83 ... 1.5)	-7.9 (-26 ... 9.9)
INM-CM4-8 historical-ssp585 (1)	0.73 (0.22 ... 1.8)	28 (-52 ... 1.2e+2)	1.1 (0.74 ... 1.4)	-9.0 (-37 ... 24)
INM-CM5-0 historical-ssp585 (1)	1.1 (0.47 ... 2.6)	-9.4 (-1.1e+2 ... 71)	0.67 (0.42 ... 1.0)	37 (-0.088 ... 68)
MPI-ESM1-2-HR historical-ssp585 (1)	0.85 (0.29 ... 2.4)	11 (-59 ... 78)	1.0 (0.70 ... 1.3)	-0.024 (-18 ... 21)
MRI-ESM2-0 historical-ssp585 (1)	1.8 (0.81 ... 3.7)	-42 (-98 ... 13)	1.4 (1.1 ... 1.7)	-31 (-53 ... -8.8)
NorESM2-LM historical-ssp585 (1)	5.0 (1.5 ... 16)	-94 (-1.6e+2 ... -22)	1.9 (1.3 ... 2.6)	-43 (-71 ... -15)
NorESM2-MM historical-ssp585 (1)	1.5 (0.47 ... 5.6)	-27 (-1.2e+2 ... 46)	1.3 (0.90 ... 1.7)	-18 (-42 ... 6.5)
CanESM2_rcp85_r1i1p1_SMHI-RCA4 historical-rcp85 (1)	0.60 (0.24 ... 1.3)	40 (-22 ... 97)	1.1 (0.93 ... 1.3)	-9.2 (-25 ... 5.9)
CNRM-CM5_rcp85_r1i1p1_SMHI-RCA4 historical-rcp85 (1)	1.5 (0.43 ... 8.0)	-29 (-1.2e+2 ... 56)	1.2 (0.79 ... 1.8)	-14 (-45 ... 14)

CSIRO-Mk3-6-0_rcp85_r1i1p1_SMHI-RCA4 historical-rcp85 (1)	0.90 (0.17 ... 5.4)	9.3 (-1.3e+2 ... 1.4e+2)	1.0 (0.56 ... 1.5)	0.35 (-41 ... 41)
EC-EARTH_rcp85_r1i1p1_SMHI-RCA4 historical-rcp85 (1)	1.7 (0.44 ... 6.1)	-34 (-1.1e+2 ... 53)	0.95 (0.55 ... 1.4)	3.6 (-27 ... 34)
IPSL-CM5A-MR_rcp85_r1i1p1_SMHI-RCA4 historical-rcp85 (1)	0.55 (0.18 ... 1.3)	51 (-27 ... 1.3e+2)	1.0 (0.67 ... 1.3)	-0.12 (-27 ... 32)
MIROC5_rcp85_r1i1p1_SMHI-RCA4 historical-rcp85 (1)	2.4 (0.54 ... 15)	-71 (-1.9e+2 ... 53)	1.7 (1.1 ... 2.7)	-47 (-85 ... -10)
MPI-ESM-LR_rcp85_r1i1p1_SMHI-RCA4 historical-rcp85 (1)	1.4 (0.45 ... 4.0)	-34 (-1.2e+2 ... 61)	1.5 (1.1 ... 1.9)	-39 (-72 ... -6.0)
NorESM1-M_rcp85_r1i1p1_SMHI-RCA4 historical-rcp85 (1)	0.70 (0.15 ... 2.8)	33 (-92 ... 1.6e+2)	0.78 (0.49 ... 1.2)	19 (-17 ... 51)
GFDL-ESM2M_rcp85_r1i1p1_SMHI-RCA4 historical-rcp85 (1)	5.6 (1.1 ... 36)	-1.0e+2 (-2.0e+2 ... -6.8)	1.1 (0.58 ... 2.1)	-5.8 (-42 ... 26)

6 Hazard synthesis

For the event definitions described above, low rainfall and effective precipitation during the December to February season over the region, we evaluate the influence of anthropogenic climate change by calculating the probability ratio and the change in intensity. We do this using both observations-based data products and climate models. Models which do not pass the evaluation tests described above (section 4) are excluded from the analysis. The aim is to synthesise results from models that pass the evaluation along with the observations-based products, to give an overarching attribution statement.

Figures 7- 10 show the changes in probability and intensity for four and two observations-based data products respectively (blue) and models (red). Before combining them into a synthesised assessment, a term to account for intermodel spread is added (in quadrature) to the natural variability of the models. This is shown in the figures as white boxes around the light red bars. The dark red bar shows the model average, consisting of a weighted mean using the (uncorrelated) uncertainties due to natural variability plus the term representing intermodel spread (i.e., the inverse square of the white bars). Observation-based products and models are combined into a single result in two ways. Firstly, we neglect common model uncertainties beyond the intermodel spread that is depicted by the model average, and compute the weighted average of models (dark red bar) and observations (dark blue bar): this is indicated by the magenta bar. As, due to common model uncertainties, model uncertainty can be larger than the intermodel spread, secondly, we also show the more conservative estimate of an unweighted, direct average of observations (dark red bar) and models (dark blue bar) contributing 50% each, indicated by the white box around the magenta bar in the synthesis figures.

For both variables the observation-based products show a wettening trend (blue bars), that is quite large in particular for rainfall alone even though uncertainties are high and thus render the trend not statistically significant. While all observation-based products show a wettening the trends are not homogenous across the region and also differ between data products. The confidence in this finding with respect to the size of the trend is thus low. Previous studies have however also shown a slight wettening with global warming in the DJF season while other seasons are dominated by drying (Onyutha, 2018).

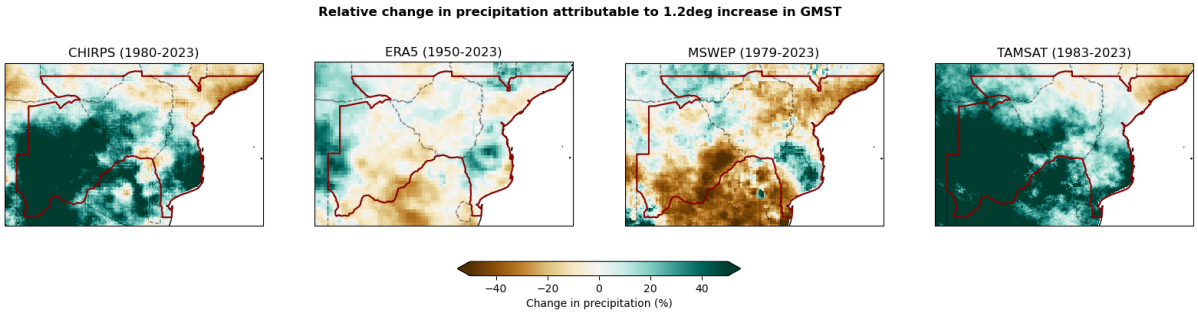

Figure 6. Relative change in precipitation *with respect to GMST per gridpoint in different observation-based data products over southern Africa.*

None of the climate models that pass the evaluation replicate this observed wettening but show consistently almost no change. A small number of models show a drying trend but overall there is no significant change in either direction. This is not only true for precipitation but also for effective precipitation. In contrast to other regions (East Africa, West Asia) we thus do not find an increase in drought severity with the increase in temperatures for this particular region and season.

When repeating the analysis comparing the present climate at 1.2C warmer than pre-industrial with a future 0.8C warmer climate the results are very similar to comparing past with present and show no significant increase or decrease in the likelihood and intensity of the DJF drought in the two variables, precipitation and effective precipitation.

In summary, our analyses show that El Nino significantly increases the likelihood of such a drought to occur, while climate change does not emerge as the significant driver influencing the assessed drought in the affected countries.

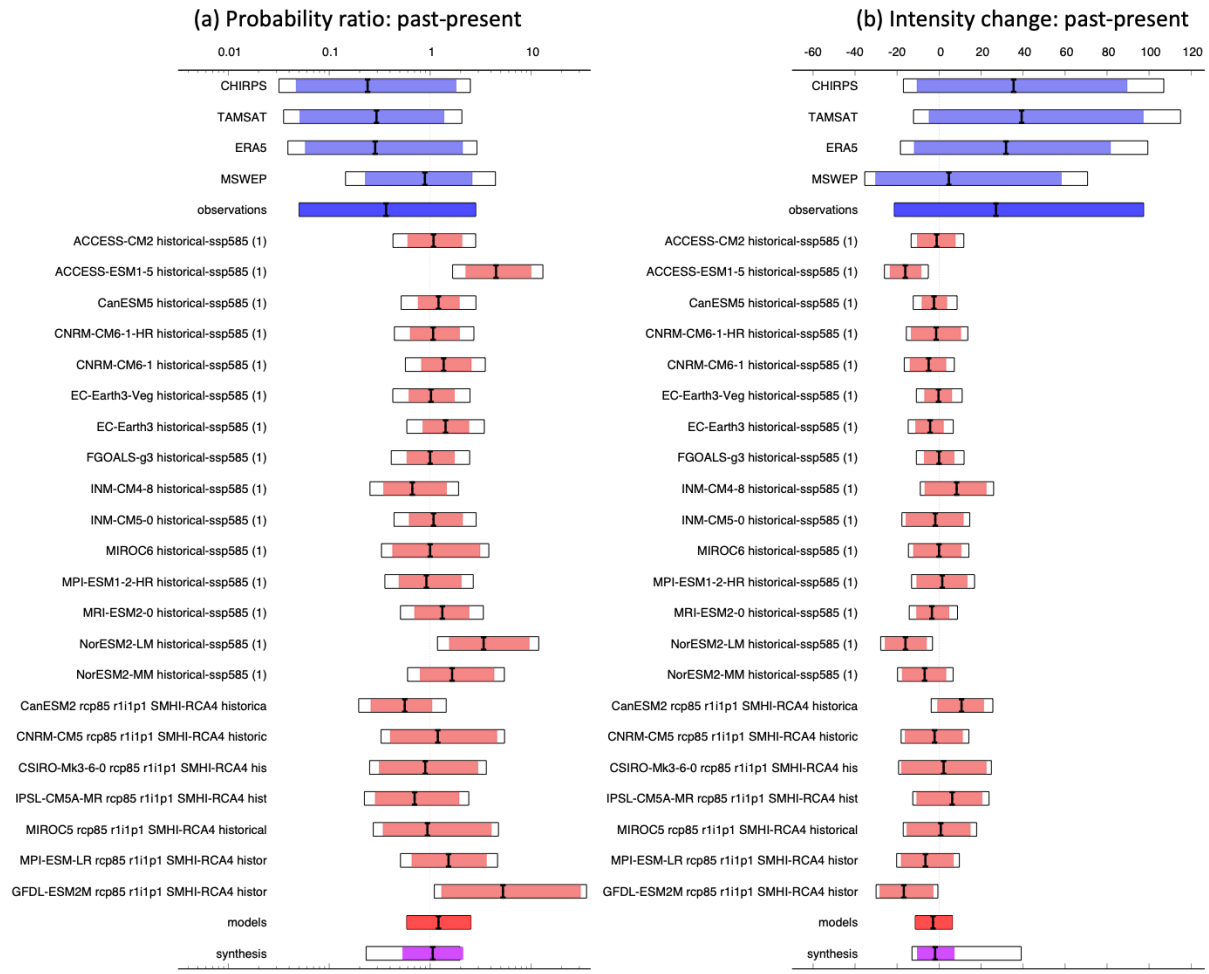

Figure 7. **(a)** ***Synthesis of probability ratios*** *(**left**) and intensity changes (%; **right**) when comparing the return period and magnitudes of the DJF rainfall over study region in the current climate and a 1.2°C cooler climate.*

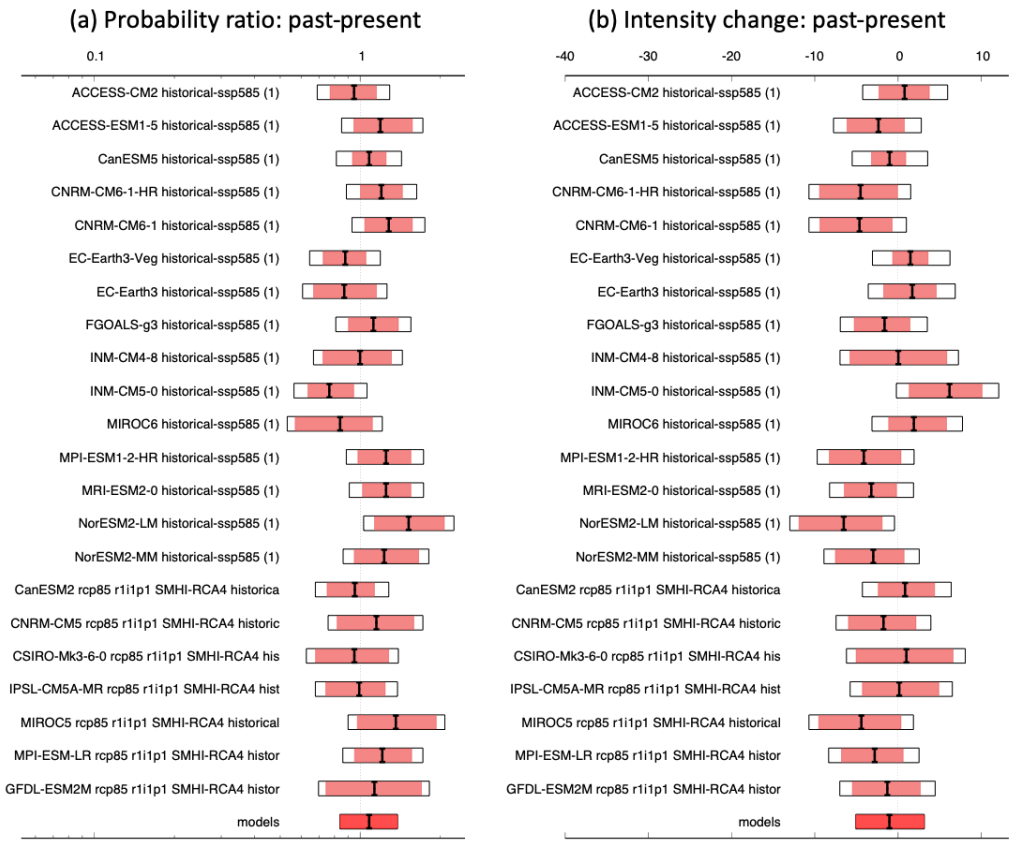

Figure 8. **(a)** ***Synthesis of probability ratios*** *(**left**) and intensity changes (%; **right**) when comparing the return period and magnitudes of the DJF rainfall over study region in the current climate and a future 0.8°C warmer climate*

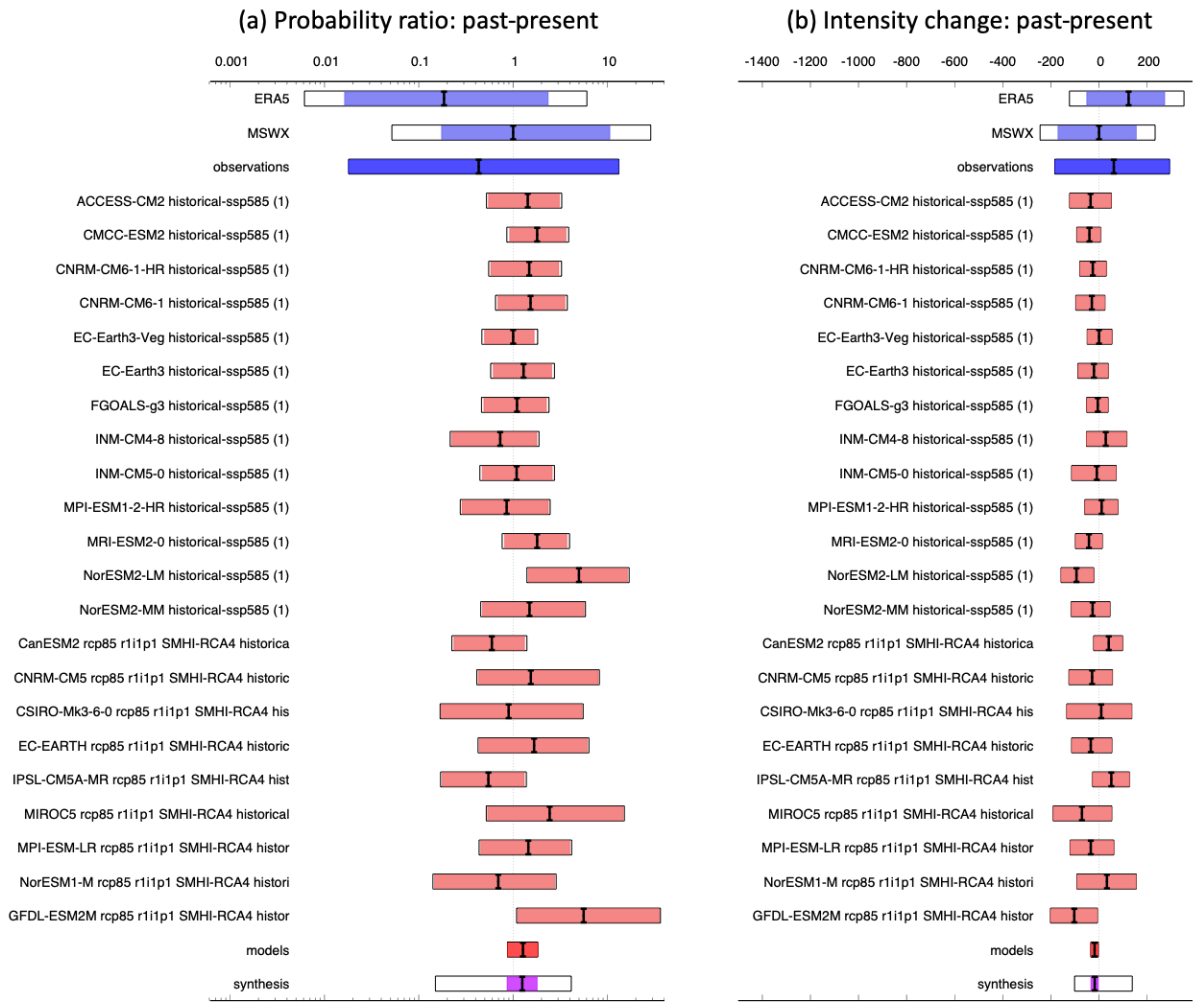

Figure 9. (**a**) ***Synthesis of probability ratios*** *(**left**) and intensity changes (%; **right**) when comparing the return period and magnitudes of the DJF effective rainfall over study region in the current climate and a 1.2°C cooler climate.*

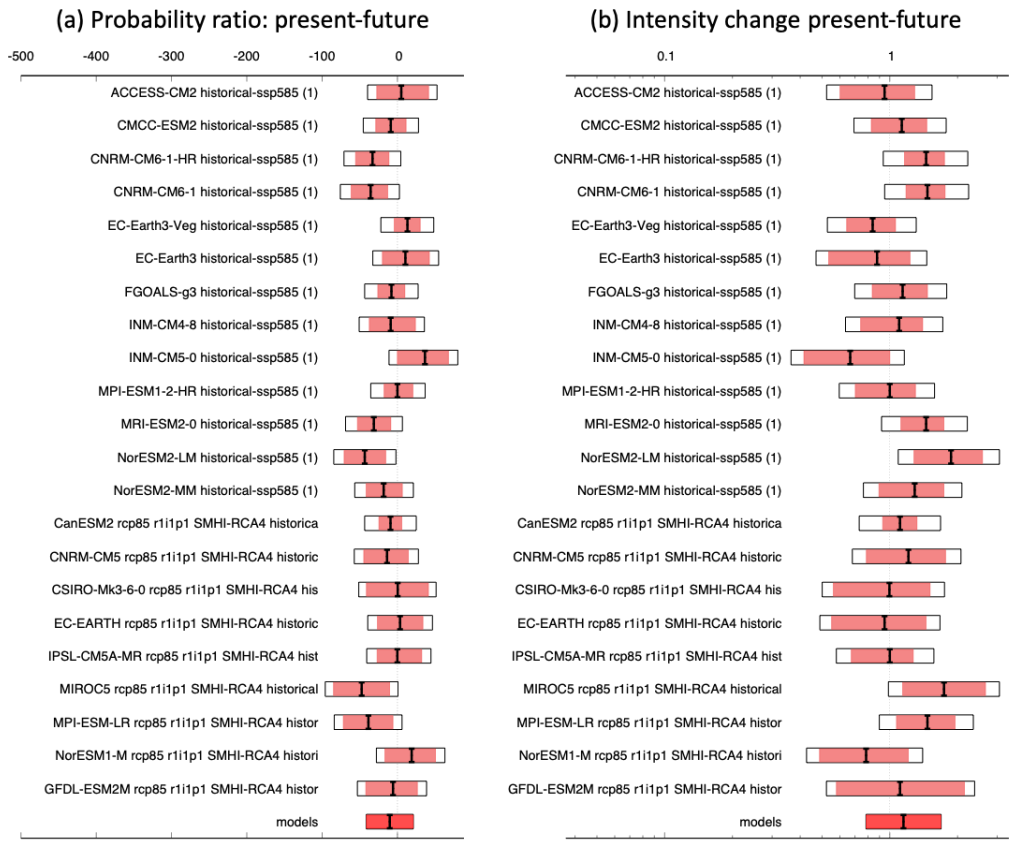

Figure 10. **(a)** ***Synthesis of probability ratios*** *(**left**) and intensity changes (%; **right**) when comparing the return period and magnitudes of the DJF rainfall over study region in the current climate and a future 0.8°C warmer climate*

7 Vulnerability and exposure

In this section, we explore the factors that increased or decreased the propensity of people and systems to be impacted by the lower-than-normal rainfall in the southern Africa region. This analysis focused on four countries in southern Africa, but aside from their geographic proximity, they are vastly different countries in many ways. For example, using the Human Development Index (HDI) as an imperfect indicator of differences in development, Botswana is categorised as having high human development whereas Zambia, Zimbabwe, and Mozambique are categorised in the medium development category (UNDP, 2024). Another example is that there is a history of conflict and violence in northern Mozambique that can amplify the impacts of an extreme drought (see e.g. UNHCR, 2020). Although security challenges in Mozambique have improved and displaced groups are returning to their areas of origin, the drought in parts of central Mozambique as well as other climate and extreme weather events have the potential to dial back these gains (Sithole, 2024; Jamie et al., 2022). In contrast, violent conflict is largely not a factor in Botswana or Zambia. Further, the countries' economies are different, have different governance systems and policies, and different infrastructure and services, which have an impact on the extent to which the lack of rainfall has an impact on people. The following sections synthesize some of the relevant factors and highlight differences and similarities between countries' vulnerability to this drought.

7.1 Compounding events

The current drought in Southern Africa during the traditional growing season for key staple crops such as maize, co-occurs with high pre-existing levels of vulnerability and exposure. Drivers of this include persistent high food prices, ongoing economic challenges, livestock and crop pests and diseases and ongoing recovery from preceding shocks (ACAPS, 2024; IPC, 2023). For example, Zambia is still recovering from widespread floods in 2023, and an ongoing Cholera outbreak in peri-urban centres across Zambia and Zimbabwe severely constrains response capacity (IFRC 2023; 2024a; 2024b; USAID, 2024). The outbreak of Cholera in Zimbabwe and Zambia early in 2024 is linked to floods followed by water shortages, exacerbated by limited access to water and sanitation, exemplifying the combination of non-climate and climate factors driving risk to human health (IFRC, 2024a; 2024b). In Zambia, USAID notes ongoing needs related to malnutrition in children and broad based food insecurity particularly in refugee camps (USAID, 2024). While Zimbabwe had an estimated 2.6 million people including 1.7 million children in need of urgent humanitarian aid as of 2024 and due to the combined impacts of drought, floods, regional migration and cholera outbreak (UNICEF, 2024). In Mozambique, cyclone Filipo has increased local needs for food, clean water, sanitation, health and shelter (IOM, 2024). Finally, the Botswana Vulnerability Assessment Committee report of July 2022, estimated nearly 37,000 people will need food assistance in 2023 due to various hazards. Additionally, long term needs in the country continue to be spread across food security and livelihoods, disaster risk reduction, health and water, sanitation and hygiene as well as climate change adaptation and environmental protection (IFRC, 2024). Although the government of Zambia has declared a national disaster, it stands to be seen whether directing all systems towards drought response will yield a successful outcome in this context of existing and cross sector humanitarian dependency (Mutsaka and Imray, 2024).

Before the 2023/2024 rainy season (NDJFM) in Southern Africa, traditionally the main planting and harvesting period for staple crops such as maize, food insecurity levels were already high. For example in Zambia, 17% of the population was already estimated to face IPC Phase 3 (crisis) or higher food insecurity levels, due to high costs of agricultural inputs, the floods in 2023 and several crop pests (fall armyworm and cassava brown streak) (IPC, 2023). Notably, the 2022/2023 season saw a maize surplus, yet this national carry-over stock could not cushion current food requirements and food prices remained high, mainly driven by global price shocks such as the Russia-Ukraine war (IPC, 2023). Research on the previous prolonged dry spell event in Zambia (2018-2020), indicates that access and connectivity result in highly localized food security dynamics (IWMI & RCCC, forthcoming).

7.2 Chronic and differential vulnerability

In southern Africa, vulnerability to drought in some cases is a chronic issue, yet not everyone is affected in the same way. Across Southern Africa, the most vulnerable people to drought impacts on food security and nutrition are rural populations dependent on small-scale rain-fed subsistence agriculture and livestock herding, daily wage labourers in the agricultural sector and their family members (IFRC, 2024). In Zambia and Zimbabwe, over 50% of the population is employed in agriculture (ILO, 2024). Research from past drought events in Zambia indicates that among these groups, high multidimensional poverty limits options for alternative livelihoods and more climate-smart practices (ZSA, 2023). Households depend on their harvest for food and sell surplus to the market. Throughout the year, households typically rely on various natural resource-dependent livelihoods, combining farming of maize, livestock production, fishing and crafts such as reed-mat making, which are all sensitive to reductions in soil moisture and surface water availability (IWMI & RCCC, forthcoming; Rosen et al., 2021).

There is diversity in vulnerability among small-holder subsistence farming communities. Community-based research indicates that older women living alone and young children are most affected by malnutrition during droughts, as they have limited means to search for alternative income sources or gather food (IWMI & RCCC, forthcoming; Rosen et al.. 2021). Farmers that only grow maize are also more vulnerable, as this crop is more susceptible to drought than other staple crops such as cassava, millet and sorghum. In the south and west of Zambia, the most drought-prone regions, access to irrigation and agricultural inputs is also highly limited due to financial barriers (Hambulo et al.. 2019). Gender-related barriers also make female-headed households more vulnerable, as they have more household responsibilities related to water and food production, and less access to inputs and information (IWMI & RCCC, forthcoming; Rosen et al.. 2021; Lwando, 2013). Lastly, rural farmers living further from main roads and cities face issues accessing seasonal warning information, (humanitarian) support and agricultural inputs (IWMI & RCCC, forthcoming).

Across Zambia, Botswana and Zimbabwe, drought also affects wildlife such as elephants and human-wildlife conflict (CGTN, 2024; Xinhua, 2024). As surface water sources diminish, wildlife, livestock and humans more frequently have to share water resources, and wildlife may damage crops and gardens in search of food. In Zimbabwe, elephants have died due to lack of water (Karombo, 2024). For communities living in or near national parks and regional wildlife migratory routes, wildlife damage to farmland for communities was reported during past events as a major issue, spurring innovative ways to protect crops (IWMI & RCCC, forthcoming; Subakanya et al., 2018; World Bank, 2019).

Compared to Zambia and Zimbabwe, Botswana is far less dependent on (rain-fed) agriculture, yet 70% of the rural population derives some part of their income from agriculture - especially livestock herding (CIWA, 2021). This is because only 0.5% of Botswana's land area is suitable for planting, owing to the semi-arid desert landscape covering the majority of the country (FAO, 2005; 2015). Food prices may impact food insecurity as harvests in South Africa are reduced due to the high import-dependency and specific groups living in poverty reliant on livestock herding may see their livelihoods affected (STATSBOTS, 2020). During past drought events, for example 2018, pastoralists were severely impacted because of cattle losses and recovery from past events is still ongoing (Reuters, 2018; 2019).

Vulnerability to drought impacts intersects with other socio-economic and health-related challenges in Zambia, Zimbabwe, Botswana and Mozambique. In particular, the high rates of existing malnutrition and high levels of persistent food insecurity signal structural issues in food availability, uptake, access and stability (ZSA 2020). Furthermore, malnutrition is further exacerbated for those living with HIV/AIDS (ZSA 2020). While HIV/AIDS infection rates are declining, the disease burden remains high across Southern Africa, especially affecting women (UNICEF, n.d.). In Zambia, approximately 8% of male adults (15 years or older), 13.9% of female adults are living with the disease (ZAMPHIA, 2022). Past assessments indicate that prevalence among children is 14% (UNAIDS, 2020). HIV/AIDS, drought, and malnutrition can form a vicious cycle (Mason et al., 2005).

Vulnerability to drought in Southern Africa is characterized by different challenges faced by various communities, from rural populations dependent on agriculture to those grappling with the intersection of socio-economic factors such as gender disparities and HIV/AIDS prevalence. Overall, addressing the multifaceted impacts of drought requires nuanced interventions that consider the specific chronic vulnerabilities of diverse groups, ranging from small-holder subsistence farmers to wildlife and those already burdened by existing health and socio-economic challenges across Zambia, Zimbabwe, Botswana, and Mozambique.

7.3 Water and electricity systems

7.3.1 Water and sanitation

Based on knowledge from previous droughts, there are concerns over water availability and access for affected communities (IFRC, 2024). In rural areas across Southern Africa water supply is decentralized, and households dependent on unimproved[1] sources and surface water are highly vulnerable to drought impacts on water availability and quality. In Zambia, 40% of the rural population depends on unimproved drinking water, and over half of the surveyed households have in the past experienced impacts from dry spells on water sources (ZVAC, 2022[2]). In urban areas, only 4.8% of households are dependent on unimproved sources (ZVAC, 2022). However, in informal peri-urban areas, households remain dependent on shallow wells with limited access to improved sanitation, which renders these households vulnerable to fluctuations in groundwater levels and price-spikes (Reaver et al. 2021). This difference between water access between the rural and urban population is present across Zambia, Zimbabwe, Mozambique and Botswana. In Zambia, the recent Cholera outbreak showed the challenges in WASH infrastructure and maintenance (IFRC, 2024). In rural and peri-urban areas, water and sanitation infrastructure is aging and insufficient to meet demands. The persistent low coverage of improved water supply and sanitation in Zambia is a product of challenges in cost-recovery for water utilities, and generally low investment into rural and peri-urban water supply systems, compared to urban (World Bank, 2020).

7.3.2 Electricity

As a result of the drought, important hydro-power sources in the region such as the Kariba dam, Itezhi-Tezhi, Kafue Gorge are facing water shortages, resulting in falling production. In response, power rationing, load shedding, power cuts, and increased energy imports have been implemented to address energy shortages (Reuters, 2024a). Zambia is reliant on hydropower for 85% of its electricity production, Zimbabwe for 70% (IEA, 2024). For Zambia, hydro-power production is important for the (copper) mining industry, one of the main income sources for the government (11% of GDP) (ACAPS, 2024). While precise calculations are not available yet, the major copper plant in Zambia has scaled back production due to electricity and water shortages (Reuters, 2024b). The power cuts will likely impact the industry's output, as well as the wider manufacturing sector (UNUWIDER et al. as cited by ACAPS, 2024). Loss in production may result in job losses and reduced government income (ACAPS, 2024).

7.4 Land use and land tenure changes

7.4.1 Deforestation

[1] Unimproved water sources are not protected from outside contamination (especially faecal matter). These encompass unprotected wells, springs lacking protection, water sold by vendors, bottled water (unless sourced from an improved supply for other purposes), and water delivered by tanker trucks (WHO, 2024). The JMP differentiates between unimproved sources and surface water, the latter ranking lowest on the water safety ladder (JMP, n.d.)

[2] The Zambia Vulnerability and Capacity Assessment is available through the ZVAC committee, through http://www.dmmu-ovp.gov.zm/.

While nuanced between the countries and time scales, deforestation is a major driver of environmental degradation across Zambia, Zimbabwe, and Mozambique, with significant implications for drought risk and impacts. Today, the total forest areas of Zambia, Mozambique, Zimbabwe, and Botswana are estimated to 60, 51, 45, and 26% of the countries' total land area, respectively (World Bank, 2021a; FAO, 2020a; FAO, 2020b; World Bank, 2021b).

In Zambia, an estimated 250-300,000 hectares (ha) of forest are cleared annually (Phiri, 2021). Zimbabwe also faces high deforestation rates; although this has been reduced to 262,000 ha per year from 312,900 ha on average during 1990-2000 (Bafana, 2022). Across the two countries, agricultural expansion, tobacco farming, mining and infrastructural developments, and fuelwood and charcoal production contribute to logging of woodlands (WWF, 2018; Manika, 2022). In Zambia, research shows that during times of low rainfall and associated load shedding and livelihood constraints, erosive coping strategies such as charcoal production increase, which drives more rapid deforestation (IWMI & RCCC, forthcoming).

Worst off among the countries of focus, Mozambique has lost about 37 million ha of forest over the past 40 years, which is equal to the size of Germany (de Vleeschauwer, 2019). Slash-and-burn agriculture, charcoal and timber production, urban expansion, and fires are pinned as the leading causes (WWF, 2018).

Botswana's woodland ecosystems lost 2,2 million ha in total forest area between 1990 and 2010, concentrated in its dryer regions (Statistics Botswana, 2013). In comparison, it was less than half of Zambia and Zimbabwe's current annual deforestation rate, but still comprised 17% of Botswana's total forest area. Key drivers to the loss of forest in Botswana include population growth and urban development, agricultural expansion, elephants, fires, and fuelwood and charcoal production (Mugari et al., 2020; Nichols et al., 2017; FAO & GEF, 2021).

Losses of forest at the rates recorded in Mozambique, Zambia, and Zimbabwe can not only disrupt rainfall patterns and exacerbate drought, but also threaten biodiversity and reduce the land's capacity to absorb water and slow down wind, increasing impacts of other extremes that frequently impact the area, such as cyclones and heavy rainfall (Semazzi and Song, 2001; Duku & Hein, 2021; Keddy, 2003; Mwareya, 2019). Mozambique has demonstrated a strong commitment to reduce deforestation and restore forests through policy, planning, and implementation of various initiatives. For example, the National REDD+ Strategy aims to cut deforestation by 40% and restore one million ha of forest by 2030 (World Bank, 2018; UNEP, 2018), and the Mozambique Forest Investment Plan outlines a programmatic landscape approach to sustainable forest and land management (UNEP, 2018).

The government of Zambia has also made considerable investments in addressing the drivers of deforestation. This includes having developed its National Investment Plan to reduce Deforestation and Forest Degradation (2018-2022) (Republic of Zambia, 2017), integrated afforestation as a key adaptation action in its National Adaptation Plan (UNFCCC, 2023), and implementing Africa's largest REDD+ project, the Luanga Community Forests Project (Mulungu, 2021). In 2018, the government further launched a $33 million program to promote sustainable land management and climate-smart agriculture, and diversify livelihoods (World Bank, 2018). Meanwhile, community-based initiatives like Farmer Managed Natural Regeneration have also made strides in restoring forests and advanced sustainable forest management (Phiri, 2021). In Botswana, the government has implemented a permitting system for the harvesting of more than 1 tonne of wood, and the protection of forests has been identified as a key conservation priority (Thobega, 2022). The slower deforestation rate in

Botswana compared to the other three countries of focus may suggest that its policies are effective. The same holds true in Zimbabwe, where the administration has instituted a tax on tobacco and vows to cultivate 25 million trees, yet more extensive legislation and enforcement is required (Bafana, 2022; Hlatswayo, 2023).

7.4.2 Land governance

Historically, most of rural Africa has relied on customary or "traditional" land tenure systems, where land is managed by local authorities and communities based on cultural norms, practices, and knowledge (see e.g. Alden Wily, 2003; World Bank, 1993). However, these systems have been undergoing significant changes due to factors like population pressure, urbanization, and increased demand from investors (see e.g. Cotula et al., 2009; Cotula et al., 2007; Cotula et al., 2006). Many southern African governments have sought to replace these traditional systems with more "modern" land administration frameworks based on state legislation, private property rights, and land titling/registration (Hull et al., 2019; Cotula et al., 2007). Hull et al. (2019) suggest that this is because customary tenure does not provide adequate tenure security to support long-term agricultural investments and productivity; a main reason being that such tenure systems are focused on group rights as opposed to the tenure of individuals.

In Zambia and Zimbabwe, traditional authorities are granted legal status as trustees of communal lands, however implementation has been slow (Byamugisha, 2016). Up to 20% of Zambia's dual land tenure system is held under statutory tenure, while about 80% is regulated under customary tenure governed by traditional leaders (Mandhu et al., 2019). In Zimbabwe, the weakening of traditional land governance has contributed to land degradation and environmental problems in communal areas (Braimoh & Chigumira, 2023; Republic of Zimbabwe, 2017; Mutambara, 2008). In contrast, Botswana has been more successful in formalizing customary tenure through local institutions (Byamugisha, 2016). The country has maintained a hybrid system blending traditional kgotla governance with modern land boards, though there are still tensions and lack of clarity between the two (Kalabamu, 2019). This has had mixed results, for instance allowing traditional leaders (dikgosi) to have a voice in government decision-making while failing to adequately protect the land rights of marginalized groups like the Basarwa (Flaherty, 2016). Meanwhile, Mozambique's 1997 Land Act protects the "rights of use and benefit" acquired through customary systems, while maintaining a state-owned land model (Cotula et al., 2007). While Mozambique's land laws formally recognize customary land rights and traditional management, implementation has been slow, with only 10% of communities having their lands formally delimited and recorded (Aminaka, 2023). This has led to frequent conflicts between the government, investors, and local communities (Aminaka, 2021).

Overall, the maintenance of robust traditional land governance systems, with appropriate integration into modern frameworks, appears crucial for sustainable land management and reducing drought vulnerability in southern Africa.

7.5 Household coping strategies

Households across Botswana, Mozambique, Zambia, and Zimbabwe deploy various coping strategies when faced with drought. Commonly reported actions based on past events include crop mixing, early planting, livestock sales, and finding off-farm income sources. In Zambia, research indicates that households also gather food to supplement their diets, for example eating unripe mangos, roots, and tubers (IWMI and RCCC, forthcoming). A major challenge reported in the case of Zambia, was the lack

of resources available to make changes to agricultural practices before, during and after drought periods (IWMI and RCCC, forthcoming; Mundu and Sichilima, 2020; Dumenu and Takam Tiamgne, 2020). In Zimbabwe, livestock owners in the past have turned to supplementary feeding, cattle disposal and lease grazing major the adopted strategies (Soul et al. 2022; Mugwagwa, 2016; Masendeke and Shoko, 2013). In Botswana, reports suggest agro-pastoralists are self-organizing self-help groups and access social protection support to maintain their herds (Basupi and Quinn, 2019).

Diversification of livelihoods has helped vulnerable households in the past to cope with drought impacts, especially the shift to more drought-resistant crop types such as sorghum and millet, and searching for seasonal off-farm income opportunities (Svodziwa, 2018). Diversification is commonly still highly natural-resource dependent and vulnerable to drought conditions. For example, in Botswana, agro-pastoralists are increasingly more sedentary, combining livestock herding with arable farming (Basupi and Quinn, 2019). In Zambia and Zimbabwe, temporary migration to search for off-farm income, for example piecework in factories, is a common coping strategy, especially for middle-aged women (IWMI & RCCC, forthcoming; Mugwagwa, 2016; Masendeke and Shoko, 2013).

7.6 Drought risk management

7.6.1 Early warning

Southern African countries come together every year at the Southern Africa Regional Climate Outlook Forum (SADC SARCOF) to develop regional seasonal outlooks. For the 2023/24 rainfall outlook, SARCOF-27 stated in late September 2023 that the SADC region is "likely to receive normal to below-normal rainfall for most of the period October to December (OND) 2023" (apart from northeastern Zambia, which was forecast to enjoy normal to above normal rainfall) (SADC, 2023). Further, "the period December, January and February (DJF) 2023/24 is expected to have normal to above normal rainfall" (apart from southern Zimbabwe and eastern Botswana, which could expect normal to below normal rainfall) (SADC, 2023). Following the SARCOF statements, the meteorological departments in Zambia and Zimbabwe downscale the seasonal forecast and triangulate it with available sources, including the International Research Institute for Climate and Society (IRI) and UK Meteorological Office (UKMO) (see e.g. Dube et al., 2024; IWMI & RCCC, forthcoming). However, already in July 2023, ACAPS (2023) had stated that El Niño would likely worsen global mean surface temperatures (GMST) and that droughts could worsen food insecurity.

Further, the Global Information and Early Warning System on Food and Agriculture (GIEWS) continuously monitors food supply and demand and other key indicators for assessing the overall food security situation in all countries of the world (FAO, n.d.-a). It issues regular analytical and objective reports on prevailing conditions and provides early warnings of impending food crises at country or regional level. At the request of national authorities, GIEWS supports countries in gathering evidence for policy decisions, or planning by development partners, through its Crop and Food Security Assessment Missions (CFSAMs), fielded jointly with WFP (WFP & FAO, 2009). In country-level application of tools for earth observation and price monitoring, GIEWS also strengthens national capacities in managing food security related information. Some of the key components include Crop Prospects and Food Situation, Crop and Food Security Assessment, and Food Price Monitoring and Analysis (FAO, n.d.-b; FAO, n.d.-c).

On 8 November 2023, the Famine Early Warning Systems Network (FEWS NET) warned that the strong El Nino will continue to exacerbate food insecurity across Southern Africa through at least early

2025 (FEWS NET, 2023). The week following, on 13 November, the Zambian Government published the Integrated Food Insecurity Phase Classification (IPC) report which highlighted that a total of 2.04 million people were going to face food insecurity in Phase 3 and above in the period October 2023 and March 2024 (IPC, 2023a). The common drivers of food insecurity included climate-related shocks, Cassava Brown Streak Disease (CBSD), fall armyworms, and economic decline. For the same time period, Mozambique's IPC report estimated that 3.3 million people would be in need of humanitarian assistance, of which 220,000 are in Phase 4 (ICP, 2023b).

Research by IWMI and RCCC (forthcoming) suggests that for previous dry spells in Zambia, communities have also relied heavily on indigenous early warning signs, including high temperatures and strong winds, locust invasions, and vegetation dynamics changes such as abundance of mango, *mukononga* and the *echika* fruit, and little to no flowering of rose wood tree, the African custard apple/*malolo*, and Dialium Angolese/*muhamani*. These signals have informed local communities' decision-making for the timing of planting and harvesting. However, it is unclear whether and to what degree such early signs informed communities' agricultural practices in connection to this event.

7.6.2 Anticipatory action

In Zambia, one of the first countries to integrate anticipatory approaches into its disaster risk management, dozens of actors operating in the country now support early action for weather and climate extremes including drought (Anticipation Hub, n.d.; ZRCS et al., 2021; IFRC, 2020). These notably include Start Network, the Zambian Red Cross Society (ZRCS), and the Food and Agriculture Organization of the United Nations (FAO), who have each developed a mechanism to prevent and reduce expected impacts associated with drought and food insecurity. Following the 2023 IPC report published in November, ZRCS started distributing multi-purpose food to 2,000 food insecure households in the Western Province and donated 10,000 of liquid chlorine to the Ministry of Health for distribution and water treatment throughout Cholera hot spot communities in December (IFRC, 2024). Other early actions included the dissemination of early warning messages centered on water, sanitation and hygiene (WaSH), food security, zoonotic diseases, protection, gender and inclusion (PGI), community engagement and accountability (CEA). 50 National Disaster Response Team members were trained in preparation for deployment (IFRC, 2024).

Zimbabwe and Mozambique have also formalized anticipatory mechanisms for drought, while Botswana is yet to do so. In Zimbabwe, early actions outlined in the Early Action Protocol include disseminating early warning messages, distributing drought tolerant seeds, livestock dosing, livestock support, multi-purpose cash transfers, school supplemental feeding, in-kind assistance, and awareness raising activities (IFRC, 2022; Anticipation Hub, n.d.). In anticipation of this El Nino-aggravated drought, the Zimbabwe Red Cross Society was allocated 366,878 CHF from the International Federation of Red Cross and Red Crescent Societies (IFRC)'s Disaster Response Emergency Fund (DREF) to roll out its first set of early actions (Anticipation Hub, 2023). Early warning messaging, distribution of drought-tolerant seeds, and livestock vaccination was carried out across five wards in the Binga District (IFRC, 2023).

Supported by the Red Cross Red Crescent Climate Centre and 510 Initiative of the Netherlands Red Cross, an Early Action Protocol (EAP) for drought in Mozambique, its third EAP, is still under development since 2020. In Mozambique, it was the first time an anticipatory action framework was activated for drought, and it targeted five districts across the Gaza Province, including the distribution of drought resistant seeds, rehabilitation of water stations, and cash transfers (FEWS NET, 2023;

UNOCHA, 2024). FAO, World Food Programme (WFP), Instituto de Comunicação Social (ICS), Ministério da Agricultura e Desenvolvimento Rural (MADER), Instituto Nacional de Meteorologia (INAM), and Instituto Nacional de Gestão e Redução do Risco (INGD) reached about 270,000 people with early messages; INGD, WFP and FAO distributed drought-tolerant seeds to over 3,000 households; and Instituto Nacional de Acção Social (INAS) and WFP have carried out cash transfers for nearly 12,000 households (MZN 2,500 per household) over a three month period (FEWS NET, 2024). After action reviews will help assess to what degree these early actions were effective for reducing impacts for vulnerable groups.

7.6.3 Response

On 29 February, the Zambian government declared a drought disaster, calling for local and international support (IFRC GO, 2024). Subsequently, the government increased the price at which it buys maize from farmers, an effort to support farmers, and announced plans to import and ration electricity to sustain the economy and industries, the mining sector in particular, which has been impacted by reduced hydropower generation (IFRC GO, 2024; ACAPS, 2024). On 4 March, the Office of the Vice President and Disaster Management Mitigation Unit (DMMU) called for a consultative meeting with relevant stakeholders to coordinate a multisectoral emergency response to the over one million affected households (IFRC, 2024). A month after the President of Zambia had declared a drought emergency, on 22 March, a six-month DREF allocation of 750,459 CHF was made by the IFRC to the Zambian Red Cross Society (ZRCS) (IFRC, 2024). At this time, another DREF-funded response was already in place to address the ongoing Anthrax and Cholera outbreaks, as well as a Cholera Emergency Appeal. Coordinating between these responses through the Incident Management Systems (IMS), the ZRCS carried out actions in the sectors of WaSH, CEA, risk communication and community engagement (RCCE), public health in emergencies, information management, and planning, monitoring, evaluation and reporting (PMER) (IFRC, 2024). Working closely with the Zambian government, UNICEF (2024) rolling out a host of measures, including building capacity among community health centres and workers to prevent malnutrition, procuring and pre-positioning supplies for prevention and treatment of malnutrition, supporting coordination of the nutrition response at sub-national and national levels, and providing and repairing emergency water supply and water treatment chemicals while drilling new water sources.

On 3 April, Zimbabwe declared the drought a national disaster, requesting $2 billion for aid as millions go hungry (The Guardian, 2024). Two days later, the government, through the Ministry of Lands, Agriculture, Fisheries, Water and Rural Development (MLAFWRD), met with the Food and Agriculture Organization of the United Nations (FAO) to assess the food security situation and outlook (FAO, 2024). Their resulting action plan outlines short and long term interventions spanning open data, early warning, anticipatory action, and emergency response. The United Nations International Children's Emergency Fund (UNICEF) has also scaled up its existing response in the country, focusing notably on life-saving assistance, mainstreaming of social and behavioral change, gender equality and prevention of sexual exploitation and abuse (UNICEF, 2024).

In Mozambique, the government and partners in the Food Security Cluster have assisted over 541,000 people with food distribution, roughly half of which in the Cabo Delgado Province alone (FEWS NET, 2023). Co-lead of the Food Security Cluster in Mozambique, FAO (2024) outlines six priorities to rebuild and restore livelihoods, enhance households' food security, and ensure anticipatory and emergency actions reach those most impacted and at risk. These include, for example, providing small livestock, restoring fisheries' value chains, and pre-positioning resources.

The government of Botswana have taken several steps in response to the drought in 2024, including increased drought relief programmes and expanded the Ipeleng public works programme to provide employment for 10,000 people and the Temo Letlotlo programme which provides 100% subsidies to micro-scale farmers (Tebogo, 2024). Botswana also introduced an animal feed subsidy to help farmers produce livestock feed, urged farmers to maintain a moderate number of cattle to avoid land degradation, and increased the number of boreholes in wildlife parks to enhance water access for animals (Tebogo, 2024). The humanitarian response in Botswana is focused on providing critical agricultural inputs, ensuring water access among livestock, protecting aquaculture and fisheries, as well as promoting climate-smart agricultural practices to support communities in becoming more resilient when faced with drought (FAO, 2024).

7.6.4 Social protection

The countries of focus have several social protection programmes in place to help populations cope with stressors and reduce vulnerability. In Zambia, these notably include the Social Cash Transfer (SCP) Program and Farmer Input Support Programme (FISP), which are aimed at providing a non-contributory payment of money to individuals and households facing extreme poverty (Republic of Zambia, n.d.) and enhancing agricultural productivity and supporting small-scale farmers (Republic of Zambia, 2023), respectively. Similarly, Zimbabwe has the National Harmonized Social Cash Transfer (HSCT) programme, providing unconditional cash to food-poor and labor-constrained households (The Transfer Project, n.d.). While Zimbabwe is one of the countries in Africa with the lowest spending on social protection, at under 0.5% of its GDP (UNICEF, 2021), the government is providing cash support through the National Action Plan for Orphans and Vulnerable Children (NAP OVC) as well as social assistance programs aimed at financially supporting and providing food security, nutrition, and healthcare assistance to the poor (de Arruda, 2018). In contrast, considered a regional leader in social protection investment, Botswana's social protection system is relatively comprehensive, having implemented over 30 programmes through 10 different government bodies (Ntseane & Solo, 2023; UNICEF, 2019; Maundemi & Mupedziswa, 2017; Tesliuc et al., 2013). These include the Ipelegeng public works programme, first introduced as a drought relief programme over 40 years ago; Destitute Persons Program; and the non-contributory pension, among others (Guven et al., 2022; Republic of Botswana, 2020). Despite considerable investments and efforts to harmonize and consolidate its social protection system, there are notable gaps in their coverage (Republic of Botswana, 2020). For instance, the 2017 Botswana Demographic Survey suggested a prevalence rate of people living with disabilities to about 4.2% of the population (~110,460 people), but the Disability Cash Transfer programme currently only reaches 8,000 people (Republic of Botswana, 2020).

In Mozambique, the key programmes are the Basic Social Subsidiary Programme, Direct Social Action Programme, Productive Social Action Programme, Social Welfare Services Programme, and Institutional Care; all implemented by the National Institute of Social Action under the Ministry of Women and Social Action. To further strengthen the social protection system in the country, the government has developed the National Basic Social Security Strategy, and are making its programmes shock responsive and scalable by integrating social protection into anticipatory action mechanisms (Tomás et al. 2022; IPC-IG, 2016). These developments are still a work in progress, as are similar commitments in Zambia proclaimed at the 2023 Social Protection Week (ILO, 2023).

V&E conclusions

Multiple drivers contributed to the currently high, and rising, food insecurity and malnutrition levels. The drought is compounded by pre-existing vulnerabilities including high food prices, economic challenges, livestock and crop pests and diseases, and ongoing recovery from previous shocks like floods and Cholera outbreaks. Chronic vulnerability to drought disproportionately affects rural populations dependent on small-scale rain-fed agriculture and livestock herding, as well as marginalized groups like female-headed households and those living with HIV/AIDS. High deforestation rates are a major driver of environmental degradation across Mozambique, Zambia, and Zimbabwe, exacerbating risk and impacts associated with drought.

Countries in the region have varying levels of development, infrastructure, and governance systems that impact their ability to respond to the drought, with Botswana generally showing more evidence of resilience than Zambia, Zimbabwe, and Mozambique. Maintaining robust traditional land governance systems with appropriate integration into modern frameworks appears crucial for sustainable land management and reducing drought vulnerability to southern Africa.

Given ENSO is largely driving the drought in southern Africa, the impacts on food security and livelihoods shows that people are vulnerable to shifts in rainfall regardless of the cause, and with the addition of other compounding events (e.g. extreme rainfall, pests etc.) the impacts only grow. Climate change in this case could be thought of as an additional stressor that could further stretch people's ability to cope. Effective early warning systems, anticipatory action, and coordinated emergency response efforts are in place, and could be further strengthened by commitments for shock responsive social protection systems.

Data availability

Almost all data are available via the Climate Explorer.
%FOR DATA THAT ISN'T, data is available upon request, CONTACT...:

Validation tables

%only for large ensembles if not totally shown in sect 4.

References

All references are given as hyperlinks in the text.
References - make sure you put all references in as hyperlinks when writing above sections

Appendix

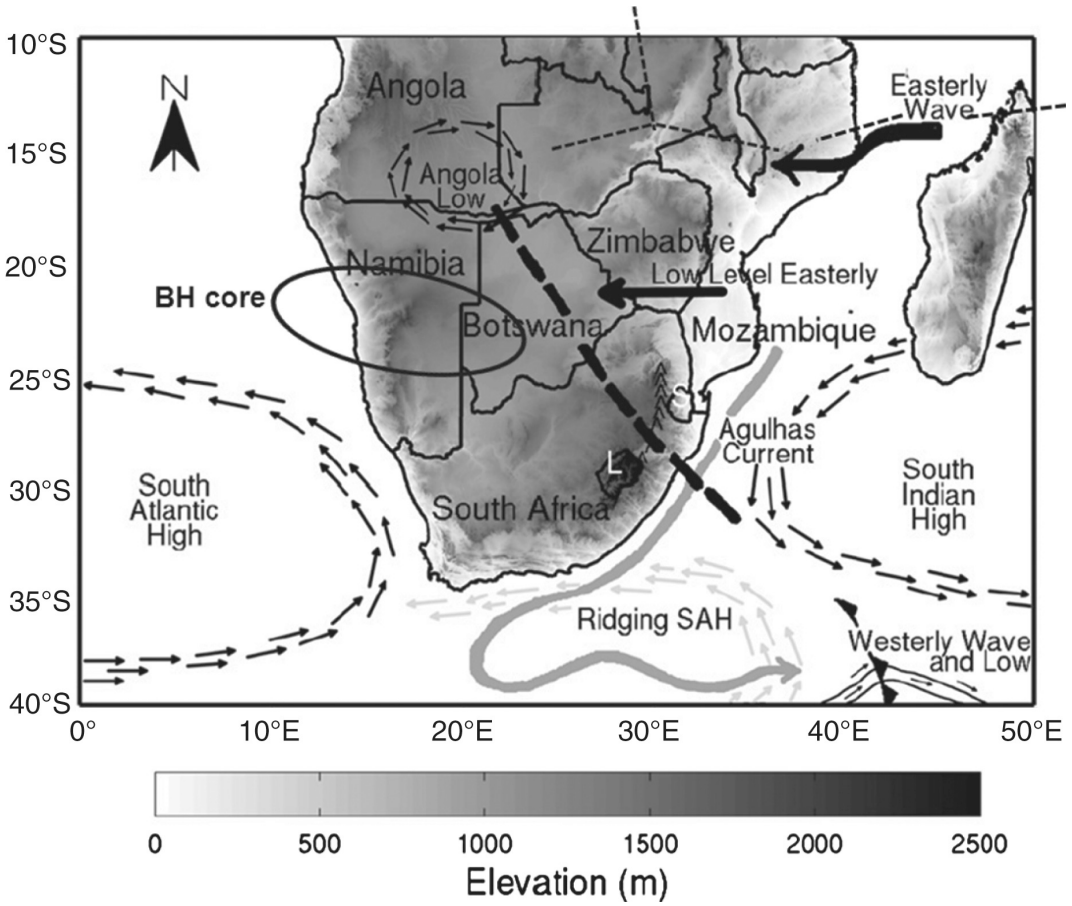

Figure A1 - Main circulation features over Southern Africa during austral summer (Reason, 2017)